Soil Dynamics and Earthquake Engineering 160 (2022) 107329

Contents lists available at ScienceDirect

Soil Dynamics and Earthquake Engineering

journal homepage: www.elsevier.com/locate/soildyn

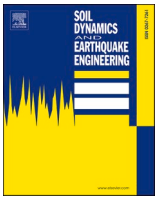

Effect of strain history on the monotonic and cyclic response of natural and reconstituted silts

Ali Dadashiserej, Amalesh Jana, Armin W. Stuedlein, T. Matthew Evans *

Oregon State University School of Civil and Construction Engineering, 101 Kearney Hall, Oregon State University, Corvallis, OR, 97331, USA

A B S T R A C T

The effect of strain history on monotonic and cyclic response of intact and reconstituted, low and high plasticity silt deposits have been investigated through a series of constant-volume, staged, stress- and strain-controlled cyclic direct simple shear tests. In many cases the specimens subjected to stress-controlled loading exhibited a progressive increase in cyclic resistance due to beneficial effects of increased density following post-cyclic reconsolidation, apparent pseudo-overconsolidation and presumably increased lateral stresses. Such effects outweighed the detrimental effects of fabric destructing as a result of the prior strain history. However, some specimens exhibited an inconsistent evolution of cyclic resistance when assessed using different shear strain cyclic failure criteria. Symmetric accumulation of shear strains in earlier shearing stages did not consistently result in an increasing trend in the post-cyclic resistance; additionally, increases or decreases in cyclic resistance can occur in subsequent shearing stages depending on the amplitude of the maximum shear strain. Staged, strain-controlled tests were used to investigate the cyclic soil response to small and large shear strains, the latter of which caused a reduction in the cyclic resistance of overconsolidated (OC) silt specimens in the following loading event, confirmed using shear wave velocity, V_s, measurements which indicated substantial fabric disturbance following the large strain event. In contrast, normally-consolidated (NC) and OC specimens subjected to multiple stages of small cyclic shear strain exhibited progressive increases in V_s, the magnitude of which varied with stress history. The increase in cyclic resistance in the NC specimens was related to increased pseudo-overconsolidation following reconsolidation. The monotonic undrained shear strength of all silt specimens subjected to staged cyclic loading increased following post-cyclic reconsolidation; the increase in strength and changes in volumetric tendencies are governed by the magnitude of post-cyclic reconsolidation and changes in soil fabric inferred from V_s, respectively.

1. Introduction

The effect of pre-shaking on the cyclic resistance of natural soil deposits in future earthquakes and storm events continues to concern practitioners and researchers in view of mainshock-aftershock, multi-mainshock earthquake sequences and wave action on offshore gravity platforms, respectively. The Canterbury Earthquake Sequence provides a recent example of the consequences of such geological phenomena [1,2], however, the effect of strain history on the seismic performance of soils has been identified some four decades earlier. Observations following earthquakes suggest that multiple successive events may or may not increase cyclic resistance of a soil deposit in future events. Kuribayashi and Tatsuoka [3] reported that a sand deposit at a single site re-liquefied during four successive earthquakes in northeast Tokyo, Japan, from 1894 to 1931. However, the natural pre-shaken silty sand deposit at the Wildlife Site in Imperial Valley, California, exhibited higher liquefaction resistance for shaking events subsequent to the initial liquefaction episode [4–6].

The effect of strain history on the cyclic resistance of granular soils has been investigated through systematic laboratory element studies [7–12], physical model tests [6,13,14], and numerical simulations [15,16]. Researchers have shown that regardless of the specimen preparation method, a single pre-shearing event may improve or degrade cyclic resistance for the following events, depending on the shear strain amplitude, γ, and the number of loading cycles, N [7,8,10,17]. Finn et al. [7] defined a single amplitude threshold shear strain for sand specimens (i.e., $\gamma_{SA} = 0.5\%$) below which pre-shearing improves cyclic resistance due to increased interlocking of the particles and removal of local instabilities at the grain-to-grain contacts. However, large pre-shaking resulted in a significant loss in resistance and larger excess pore pressures in subsequent shaking events due to the development of microstructural (i.e., fabric) anisotropy, fabric rearrangement, and the destruction of soil fabric that had developed due to aging, cementation, and biogeochemical activities, and the corresponding reduction in the initial lateral stresses [7,11,18,19].

In contrast to the effect of a single pre–shaking event, sand deposits subjected to multiple shaking events may exhibit a net progressive increase in cyclic resistance over geologic time [6,20,21]. El-Sekelly et al. [6] performed a series of centrifuge experiments on a young silty sand deposit subjected to 66 shaking events with each relatively strong

* Corresponding author.
E-mail address: matt.evans@oregonstate.edu (T.M. Evans).

https://doi.org/10.1016/j.soildyn.2022.107329
Received 22 October 2021; Received in revised form 25 April 2022; Accepted 27 April 2022
Available online 7 June 2022

pre-shaking event followed by ten small pre-shaking events, intended to simulate the seismic history of the Wildlife Site. The small pre-shaking events that did not generate significant excess pore pressure increased the cyclic resistance for the subsequent strong pre-shaking event, whereas the strong event resulted in a dramatic reduction in cyclic resistance due to the removal of the prior beneficial effects of small shakings. Similarly, the effect of episodic loadings and reconsolidation on cyclic resistance of clay deposits has been studied using element tests [22], physical modeling [23], and numerical simulations [24] for geotechnical design of offshore structures. The results indicated that preshearing improves the resistance of normally consolidated clays; however, it can have a detrimental effect on cyclic resistance of over-consolidated clays.

Whereas most of these prior studies have comprehensively investigated the response of clean or silty sand and fewer have focused on clays, very limited laboratory studies and case histories exist for nonplastic [25,26] and low plasticity silts [27] and even fewer exist for intact natural silts [28]. Price et al. [27] performed a series of staged, stress-controlled, cyclic direct simple shear (DSS) tests to examine the effect of strain history on cyclic resistance of normally- (NC) and over-consolidated (OC), reconstituted nonplastic silt (crushed silica silt, $PI = 0$) and low plasticity silt (crushed silica silt mixed with Kaolinite, $PI = 6$) specimens. NC specimens exhibited a progressive increase in cyclic resistance for subsequent shaking events, attributed to post–cyclic densification, which overshadowed the detrimental effects of soil fabric destruction resulting from the prior cyclic straining. However, OC specimens exhibited a reduction in cyclic resistance ranging from 18 to 32% following the first cyclic event despite the higher specimen density. The observed cyclic resistance degradation was primarily attributed to the destruction in soil fabric and reduction of lateral stresses resulting from its prior stress history. Soysa and Wijewickreme [25] conducted a series of stress-controlled, cyclic direct simple shear (DSS) tests to investigate the effect of pre-shearing on cyclic resistance of NC reconstituted specimens prepared from Fraser River nonplastic silt. The post-cyclic resistance progressively increased for specimens sheared to 3.75% single amplitude shear strain, γ_{SA}, whereas specimens subjected to $\gamma_{SA} > 10\%$ resulted in a significant reduction in cyclic resistance in the following events. Specimens subjected to such large shear strain amplitudes produced unsymmetrical shear stress-shear strain, τ-γ, hysteresis in subsequent loading stages which resulted in a smaller N to reach a pre-defined maximum excess pore pressure ratio, $r_{u,max}$, and shear strain failure criterion [26,29].

The limited previously-reported evolution in the cyclic resistance of reconstituted nonplastic [25,26] and low-plasticity [27] silt and intact nonplastic silts [28] suggests that further investigation into pre-straining is necessary, particularly towards understanding the role of stress history, natural soil fabric and inherent variability, plasticity index, and shear strain amplitude. This study presents the results of a systematic laboratory test program conducted to evaluate the effect of cyclic pre-straining on the response of natural and reconstituted low and medium plasticity silt specimens. Specific key questions have been identified with regard to stress-controlled cyclic tests to evaluate the cyclic resistance of natural silt due to multiple loading events: (1) does the choice of different shear strain-based failure criteria affect the evaluation of cyclic resistance? (2) does the cyclic resistance evaluated based on shear strain failure criteria and pore pressure response yield a similar outcome? (3) do symmetry of shear strain accumulation and amplitude of developed maximum shear strain affect the soil response? (4) can the shear strain-excess pore pressure relationship be used as an alternative to identify the evolution of cyclic resistance?

For the range in applied *CSR*s, vertical effective stresses, σ'_{vc}, and the properties of typical silt specimens (e.g., *PI*, *OCR*), testing under stress-controlled conditions generally necessitates the application of medium to large shear strains (i.e., larger than 0.3% [30]) during the first cycle of loading, obscuring the role of soil fabric on the cyclic response. Therefore, a series of constant-volume, staged, strain-controlled, cyclic tests with shear wave velocity measurements was conducted on reconstituted NC and OC specimens with the goal of capturing the effect of stress history, soil fabric, and shear strain amplitude on cyclic response. In addition, constant-volume, monotonic DSS tests were conducted on pre-strained reconsolidated specimens to investigate evolution of undrained shear strength of the soil due to multiple cyclic loading and reconsolidation events. The findings of this study will help to deepen understanding of cyclic response of plastic silts subjected to repeated seismic loadings.

2. Laboratory testing program

2.1. Cyclic direct simple shear (DSS) test apparatus

The tests described herein were performed using the SSH-100 cyclic DSS test apparatus manufactured by GCTS (Tempe, AZ) with loading platens retrofitted to accommodate bender element (BE) and piezoelectric disc (PD) transducers (Figs. S1 and S2 which are provided in Supplemental Online Appendix S1). The conventional cyclic DSS device uses a fixed top loading platen and a sliding base platen mounted on a series of linear bearings. Cylindrical specimens with diameter of 70 mm and a typical height of 20 mm are confined with a series of stacked rings (SGI-type) to prevent horizontal strain. A hydraulic servo-feedback controlled normal load actuator facilitates constant-volume conditions to simulate undrained response [31]. All constant-volume, monotonic and cyclic DSS tests conducted maintained the initial specimen height within 0.05% per ASTM D8296-19 [32].

The body wave measurement system consists of pairs of BE and PD transducers, an arbitrary function generator to excite the transmitting transducers, and a digital oscilloscope. Compression wave velocity, V_p, measurements were used to compare and judge the degree of saturation of natural specimens inferred from gravimetric and volumetric measurements. The shear wave velocity, V_s, measurement in the vertical direction provided an effective indication of specimen quality (e.g. Refs. [33,34]), and changes in the soil fabric of specimens subjected to cyclic loading (e.g. Ref. [6]).

2.2. Characterization of silt specimens

A systematic laboratory testing program was conducted on intact and reconstituted specimens prepared from intact thin-walled tube samples retrieved from two test sites. Site B corresponds to the Van Buren Bridge crossing the Willamette River in Corvallis, OR; Site D is located at the Port of Portland, Portland, OR. Representative soil profiles for each site (Site B: Fig. S3; Site D: Fig. S4), are provided in the Supplemental Online Appendix S1. The soil deposit at Site B consists of medium stiff to stiff, low plasticity alluvial silt (Figs. S5 and S6), which extends to an approximate depth of 4 m at borehole B-13, and ranges in depths from 7 to 10.5 m at borehole B-14, as described by Dadashiserej et al. [35]. The average CPT-based Soil Behavior Type Index, I_c, equaled 2.96 for the silt deposit measured in close proximity to B-13. The deposit at Site D consists of medium stiff, alluvial clayey silt with traces of sand and thin partings of sandy silt with an average I_c of 2.99 (Fig. S7) described by Jana et al. [36] and Jana and Stuedlein [34,37,38]. Intact soil samples were obtained in accordance with ASTM-D1587 [39] using an Osterberg piston sampler and specially fabricated, stainless-steel, thin-walled tubes having an outer diameter of 76.2 mm, area ratio of 8.4%, wall thickness of 1.5 mm, and machine-beveled inside cutting edge similar to that described by Soysa and Wijewickreme [40]. To prevent moisture loss during transportation and storage, expandable packers, plastic caps, and plastic wrap were used to seal the tube. The recovered Shelby tubes were transported in an upright condition and stored in climate-controlled environment until extrusion and specimen preparation. For each site, the soil sample was collected at or below the groundwater table. The groundwater tables vary seasonally and with

changes in the water level in the Willamette (Site B) and the Columbia Rivers (Site D); local dewatering operations also affected Site D. Explorations conducted at different times encountered the groundwater table at depths ranging from 1.0 to 3.5 m at the location of CPT-08 for Site B and 3.0–7.3 m for Site D. Effective stresses were calculated using the groundwater table depth at the time of each exploration; the groundwater table corresponds to depths of 2.4 m for Site B (at the location of CPT-08) and 4.2 m for Site D, respectively, at the time of sampling.

Reconstituted specimens were prepared using the slurry-deposition method by hydrating crushed soil using a water content, w, of twice the liquid limit for a minimum of 24 h following procedures reported by Soysa [41] following oven-drying at 85 °C and to produce uniform specimens that simulate the soil fabric of fluvial depositional environments [29,42]. The method of soil drying (i.e., air-dried versus oven-dried) for preparation of reconstituted specimens has a minor effect on the test results as soil samples were classified as silt per the Unified Classification System (USCS; Fig. 1a) with less than 20% clay sized particles determined using hydrometer analysis in accordance with ASTM D7928-17 [43], (Fig. 1b).

Samples from Site B were retrieved from boreholes B-13 and B-14 and are classified as low-plasticity silt (ML) per the Unified Soil Classification System (USCS; Fig. 1a) with average natural water contents, w_n, of 59% for B-13 and 41% for B-14, average liquid limit, LL, of 47 and plasticity index, PI, of 15 for B-13 and LL of 41 and PI of 13 for B-14, and fines contents, FC, of approximately 94% and 86% for B-13 and B-14, respectively (Table 1). Fig. 1b indicates that Site B samples consist of 14–20% clay-sized particles and about 73% silt-sized particles. Site D samples are classified as high-plasticity silt (MH) with average w_n = 75%, average LL = 70 and PI = 26, FC = 100%, with 84% silt-sized particles (Fig. 1a and b). All laboratory tests were conducted on specimens at nearly-saturated and fully-saturated conditions ($S_\gamma \geq 99.5\%$). The measured V_p (>700 m/s) and gravimetric water contents confirm the nearly fully-saturated and saturated conditions of the specimens [44,45]. The liquefaction susceptibility and potential for cyclic softening failure for specimens tested in this study were evaluated using criteria proposed by Boulanger and Idriss ([46]; BI06), Bray and Sancio ([47], BS06), and the framework suggested by Armstrong and Malvick ([48], AM16). Intact and reconstituted specimens from Sites B and D have been identified as moderately susceptible and nonsusceptible to liquefaction, respectively (BS06), while BI06 suggests that the fundamental behavior of all specimens of both sites should be clay-like, and should be assessed using cyclic softening procedures (AM16). Although not the focus of this paper, the differences in hysteretic behavior (e.g., sand-like vs. clay-like) for the low and high plasticity specimens is notable in view of the similarity in I_c.

Representative intact natural specimens were subjected to constant rate-of-strain (CRS) consolidation without back-pressure saturation following the procedure described by Landon et al. [49] to determine the compression (C_c) and swell (C_s) indices, the preconsolidation stress (σ_p'), and overconsolidation ratio (OCR). A strain rate of 0.45–0.75%/h was selected to avoid exceeding the threshold excess pore pressure ratio of 15% measured at the bottom of specimens [50]. Fig. 1c presents the representative oedometric compression responses of intact specimens from Sites B and D. The higher plasticity Site D specimen exhibited greater compressibility with a well-defined σ_p' as compared to the rounded oedometric response of the low plasticity Site B specimens (B-13 and B-14). The analysis of σ_p' using the strain energy method [51] and Casagrande construction [52] produced σ_p' of 95 and 250 kPa for Site B Groups B-13 and B-14 specimens, respectively, and 207 kPa for Site D. Given the *in-situ* vertical effective stress, σ_{v0}', calculated for each specimen and summarized in Table 1, the silts at Sites B and D are lightly-overconsolidated with average OCRs of 1.7 and 1.9, respectively. Specimen quality was evaluated using the work- and strain energy-based

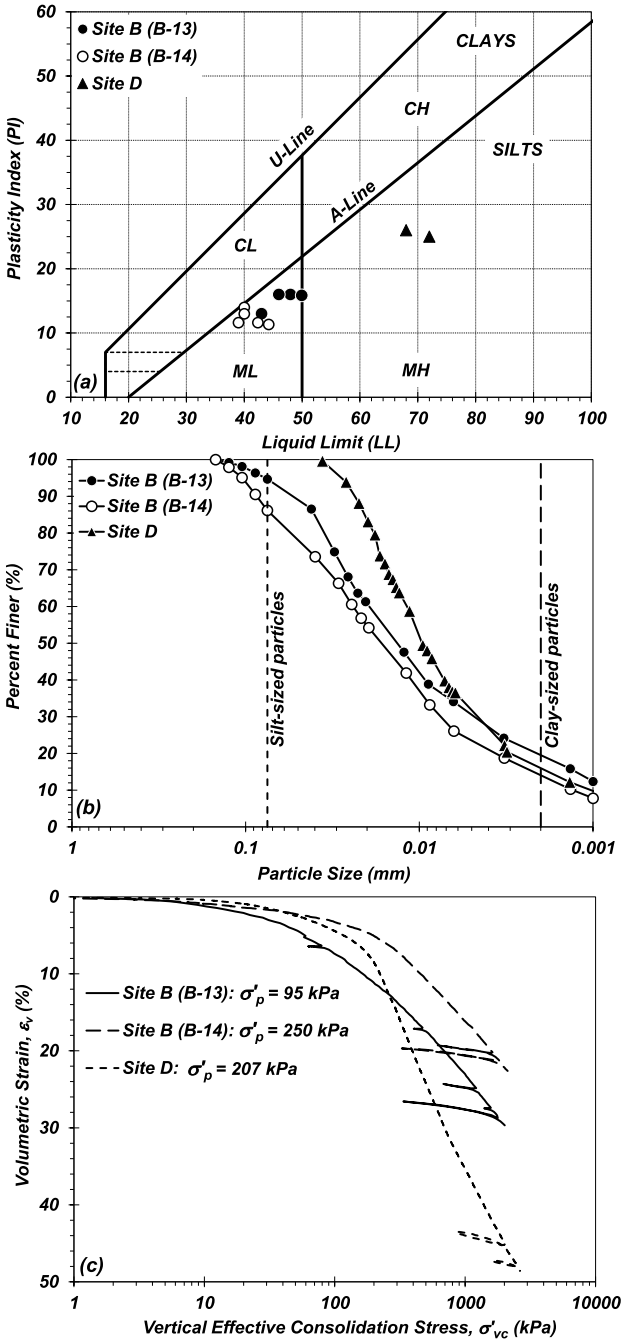

Fig. 1. Characterization of samples retrieved from Sites B and D: (a) plasticity chart, (b) particle size distributions, and (c) constant rate-of-strain (CRS) consolidation responses.

criteria proposed by DeJong et al. [53] in which the ratio of the initial recompression index to compression index, C_{ri}/C_c, and ratio of strain work-based initial recompression index to compression index, C_{rw}/C_{cw}, indicates sample quality. The calculated ratios are C_{ri}/C_c = 0.12 and C_{rw}/C_{cw} = 0.18 for B-13 specimens of Site B, C_{ri}/C_c = 0.19 and C_{rw}/C_{cw} = 0.27 for B-14 specimens of Site B, and C_{ri}/C_c = 0.13 and C_{rw}/C_{cw} = 0.11 for specimens of Site D, indicating relatively high-quality samples [53].

Constant-volume, monotonic, strain-controlled DSS tests were performed on natural, intact specimens retrieved from Sites B and D, and reconstituted specimens from Site D following the guidelines presented in ASTM D8296-19 [32] (ASTM 2019) with modification to the

Table 1
Details of test sites and material characterization.

	Site B: Willamette River Corvallis, OR		Site D: Columbia River Portland, OR
Borehole	B-13	B-14	*None*
Sample Depth (m)	2.4–3.2	8.5–9.3	9.1–11.2
Specific Gravity, G_s	2.67	2.67	2.64
Range of Natural water Content, w_n (%)	55–62	38–44	73–86
Degree of Saturation, S_r (%)	100.0	99.5–100.0	99.6–100
Average of Liquid Limit, *LL*	47	40	70
Average of Plasticity Index, *PI*	15	13	26
Unified Soil Classification (USCS)	ML	ML	MH
In-situ Vertical Effective Stress, σ'_{v0} (kPa)	50	160	98–118
Overconsolidation Ratio, *OCR*	1.8–2.0	1.4–1.7	1.6–2.2
In-situ Shear Wave Velocity, V_s (m/s)	NA[a]	NA	119–154
Laboratory Shear Wave Velocity, V_s (m/s)	85–93	168–175	121
Laboratory Compression Wave Velocity, V_p (m/s)	935–1105	862–906	1030

[a] NA = Not applicable.

consolidation procedure. The intact specimens were consolidated to vertical consolidation stresses, σ'_{vc}, equal to the *in-situ* σ'_{v0} using the recompression technique with the load maintained for at least ten times longer than the time for primary consolidation prior to shearing. The recompression technique was preferred to the SHANSEP-based mechanical unloading approach [54] for monotonic and cyclic tests owing to the potential for inducing significant reductions in void ratio should an uncertain estimate in σ'_p be exceeded (e.g., due to rounded compression curves for Site B specimens, Fig. 1c [55–58]). In addition, due to the high quality of the prepared specimens, the recompression method is expected to replicate the *in-situ* stress state condition to the high degree, confirmed through comparison of bender element- and *in-situ*-based shear wave velocities. The results of an initial sensitivity study on intact specimens from Site D indicated that differences in void ratio between the SHANSEP and recompression consolidation procedures lead to cyclic resistances from SHANSEP-type specimens that were 10–25% larger than recompression-type (see Fig. S8 in the Supplemental Appendix S1). Reconstituted Site D specimens were tested at normally consolidated and lightly overconsolidated ($OCR = 2$; hereafter referred as OC) conditions, the latter of which was performed by consolidating specimens to $\sigma'_{vc} = 200\ kPa$ and unloading to 100 *kPa*. After completion of consolidated stage as mentioned above, constant-volume shearing commenced with a strain rate of 5%/h. Fig. 2 presents the representative normalized shear stress–shear strain responses, $(\tau_h/\sigma'_{vc}) - \gamma$, and effective stress paths for the intact and reconstituted silt specimens. The Site B specimens exhibited a near perfectly-plastic $(\tau_h/\sigma'_{vc}) - \gamma$ response, whereas the Site D specimens exhibited strain hardening with undrained shear strengths, $s_{u,DSS}$, approximately 25–40% greater than the $s_{u,DSS}$ of Site B specimens.

2.3. Cyclic shear test procedures

Constant-volume, staged, stress-controlled cyclic tests with shear wave velocity measurement were performed with 0.1 Hz loading frequency to investigate the effect of strain history on cyclic resistance of intact and reconstituted specimens from Sites B and D. The specimens

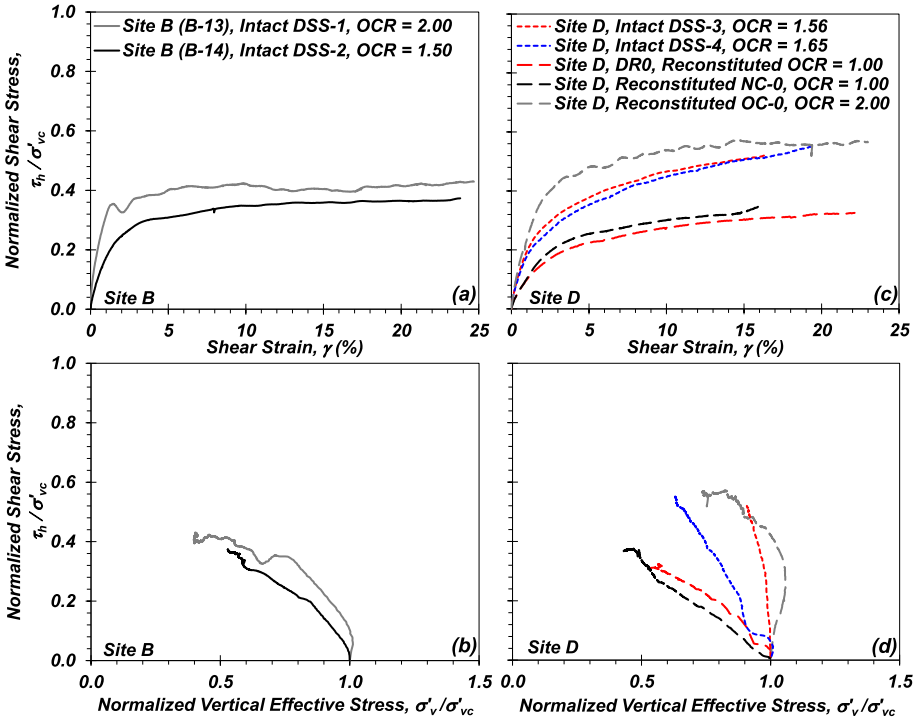

Fig. 2. Monotonic undrained DSS response of intact specimens of Site B: (a) normalized shear stress-shear strain responses, and (b) effective stress paths, and monotonic undrained DSS response of intact and reconstituted specimens from Site D: (c) normalized shear stress-shear strain responses, and (d) effective stress paths.

were subjected to constant *CSR* in successive shearing stages to isolate the coupled effects of densification resulting from post-cyclic reconsolidation and fabric destruction. Inconsistences in the evaluation of cyclic resistance were assessed based on different cyclic failure criteria including *N* necessary to achieve single or double-amplitude shear strains of 3, 3.75, and 5% (i.e., $N_{\gamma_{SA}=3\%}$, $N_{\gamma_{SA}=3.75\%}$, $N_{\gamma_{SA}=5\%}$, and $N_{\gamma_{DA}=5\%}$) and various excess pore pressure, $r_{u,max}$, responses (i.e., $N_{r_{u,max}=60\%}$ and $N_{r_{u,max}=85\%}$).

Owing to the inability of stress-controlled cyclic tests to capture the effect of soil fabric due to application of medium to large strains in the first cycle of loading and biased accumulation of shear strain during stress-controlled conditions, a number of constant-volume, staged, strain controlled, cyclic tests with shear wave velocity measurement were conducted with 0.1 Hz loading frequency on reconstituted NC and OC specimens from Site D. The goal of these strain-controlled tests was to capture the effects of soil fabric and a wide range of shear strain amplitudes on the cyclic response. Reconstituted Site D specimens were used to compare the response of soil subjected to stress-controlled and strain-controlled tests. The effects of variation in soil properties (i.e., *PI*, *OCR*, and *FC*) on cyclic response during strain-controlled tests are not considered in this study.

2.3.1. Constant-volume, staged, stress-controlled cyclic tests

Fig. 3a through 3d present schematics illustrating the staged loading protocols for the stress-controlled DSS tests consisting of multiple cyclic loading and reconsolidation phases. Following the completion of primary consolidation to $\sigma'_{vc} = \sigma'_{v0}$, the cyclic loading phase commenced under a specified cyclic stress ratio, *CSR*. Cyclic loading continued until a predefined single-amplitude shear strain, $5 < \gamma_{SA} < 20\%$, was achieved to identify the influence of the maximum shear strain amplitude, γ_{max}, on the cyclic resistance of soil for subsequent events. Following completion of the cyclic loading phase, specimens were re-centered in the DSS device and reconsolidated to $\sigma'_{vc} = \sigma'_{v0}$. The next cyclic phase commenced following dissipation of excess pore pressures and measurement of V_s, and the *CSR* applied in the subsequent shearing phase was maintained or increased depending on the evolution of cyclic resistance as a result of the previous loading.

2.3.2. Constant-volume, staged, strain-controlled cyclic test

Fig. 3e and f illustrate two loading protocols for the constant-volume,

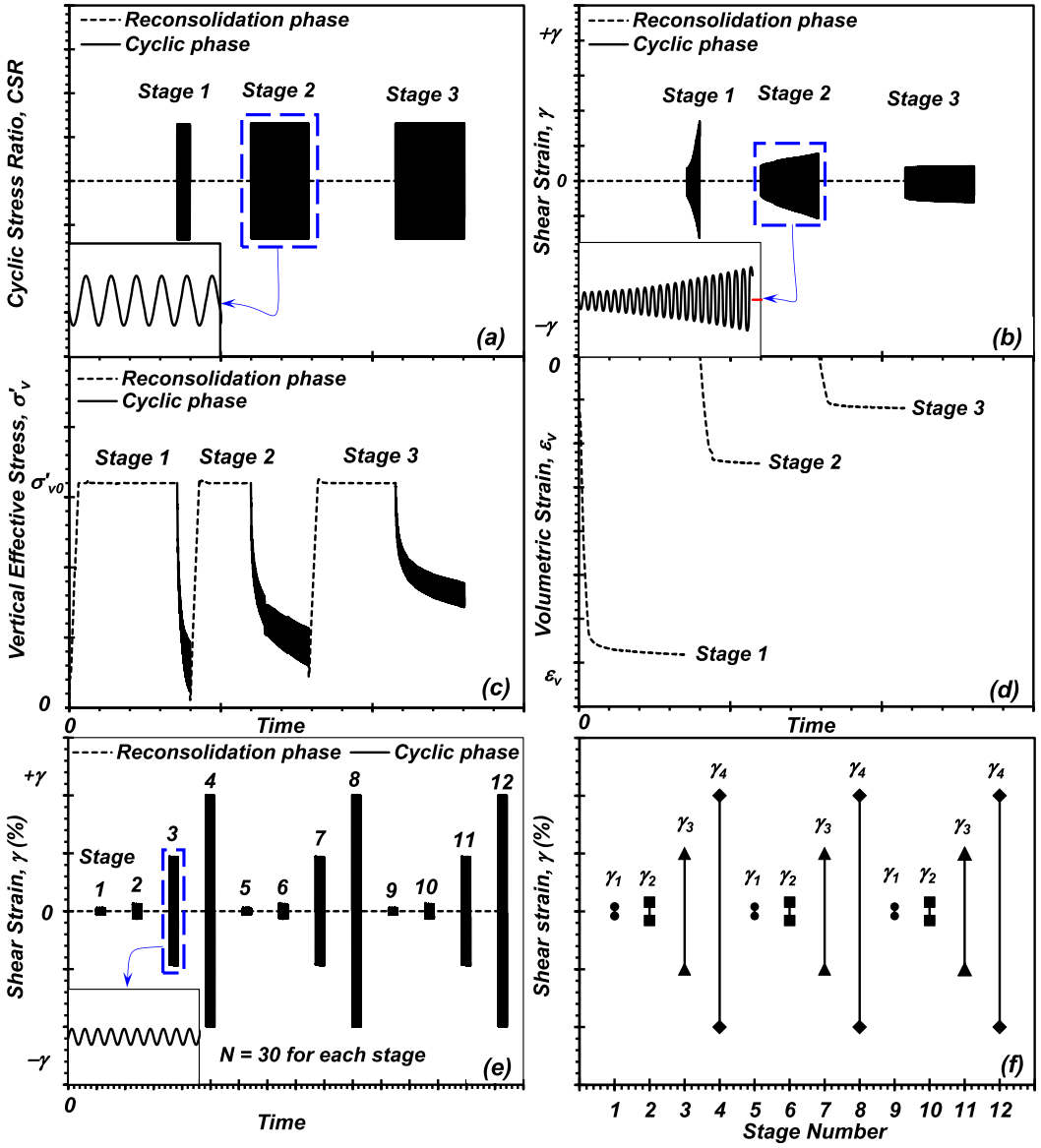

Fig. 3. Schematic loading protocols of staged cyclic DSS tests (a) stress-controlled loading and corresponding (b) shear strain (c) vertical effective stress and (d) volumetric strain time histories; (e) and (f) strain-controlled loading.

staged, strain-controlled cyclic tests which consist of three identical and repeated loading sequences at four shear strain amplitudes (12 distinct stages in total). Each sequence includes $N = 30$ cycles at each of four uniform amplitudes of shear strain: $\gamma_1 = 0.04\% < \gamma_2 = 0.08\% < \gamma_3 = 0.5\% < \gamma_4 = 1\%$ or 3%. Specimens were subjected to a reconsolidation stage following each cyclic shearing stage. The final cyclic shear stage in a given sequence corresponds to the largest shear strain amplitude where $\gamma_4 = 1\%$ is designated as small shaking (denoted S) and 3% is designated as large shaking (denoted L). The summary of the investigated factors that possibly control the cyclic response of soil for future shaking events and the corresponding metrics used to study these factors for stress-controlled and strain controlled cyclic tests are presented in Table 2.

3. Experimental test results and discussion

3.1. Constant-volume stress-controlled tests on low plasticity (Site B) silts

The results of the staged, cyclic loading of four intact, lightly-overconsolidated specimens (i.e., BU1, BU2, BU3, and BU4) and two lightly-OC reconstituted specimens (i.e., BR1 and BR2) are summarized in Table 3. The specific loading stage is denoted by the stage number (e.g., S1, S2, S3, and S4). Fig. 4 presents the multiple shearing stages for Specimen BU1 in terms of normalized shear stress-shear strain *CSR*-γ hysteresis, effective stress paths, and accumulation of r_u and γ with N for three cyclic loading stages. Following reconsolidation to $\sigma'_{vc} = \sigma'_{v0} = 160$ kPa, Specimen BU1 was initially subjected to $CSR = 0.26$ (BU1–S1) which terminated at a maximum shear strain, $\gamma_{max} = 8.5\%$ after $N = 25.5$, followed by reconsolidation and shearing in subsequent stages (i.e., BU1–S2 and BU1–S3). Fig. 4a, e, and 4i illustrate the *CSR*-γ hysteresis for BU1–S1, BU1–S2, and BU1–S3 and demonstrate the progressive increase in cyclic resistance with each loading stage, to result in $N_{\gamma_{SA}=3.75\%} = 10.7$, 47.8, and $N_{\gamma_{SA}=3.75\%} > 136$, respectively. The effective stress paths for all three stages indicate cyclic mobility with an initial contractive tendency followed by alternating dilation and contraction in loading and unloading, respectively (Fig. 4b, f, and 4j). The initial contractive tendency of the specimen decreased and gradually transitioned to a dilative tendency in the first cycle of loading as the number of loading stages increased (Fig. 4b, f, and 4j) which resulted in the generation of lower r_u in subsequent loading stages (Fig. 4c, g, and 4k). Note that at constant *CSR*, the $N_{\gamma_{SA}=3\%}$ and $N_{\gamma_{SA}=3.75\%}$ become large ($N > 100$) following reconsolidation and densification, a consistent observation in the current investigation (Tables 3 and 4). The power laws describing *CRR-N* for specimens from B-13 and B-14 are characterized with an exponent, b, of approximately 0.11 and 0.08 (Dadashiserej et al. [35]), respectively. Boulanger and Idriss [59] report the mean N for $M_w = 7.5$ in the range of about 70–200 for $b = 0.08$ to 0.11, with ground motions exceeding $N = 400$ in the former case. Thus, the N observed towards the latter stages of loading may be considered appropriate for large earthquakes.

Fig. 4d, h, and 4l indicate a reduction in the rate of shear strain accumulation with N at a constant *CSR* as the number of loading stages increased. The reduction of the specimen void ratio, e_c, because of post-cyclic volumetric strain, ε_{vpc} following reconsolidation (Table 3) and presumably increases in lateral stress [9] are responsible for the improvement in cyclic resistance. Apparently, the reduction in e_c and possible increase in lateral stress overshadowed the detrimental effects associated with the soil fabric destruction due to the prior strain history with $\gamma_{max} = 8.5$, 5.3, and 3% for BU1–S1, BU1–S2, and BU1–S3, respectively. Characterized by higher *OCR* and void ratio, and lower σ'_{vc}, intact Specimens BU2 and BU3 exhibited the same trends in cyclic resistance for similar multiple cyclic loading events (Table 3).

In contrast with Specimens BU1, BU2, and BU3, which exhibited progressive increases in cyclic resistance, Specimen BU-4 exhibited an inconsistent trend in the evolution of cyclic resistance (Fig. 5a, e, 5i, and 5 m). For example, the cyclic resistance of the more dense Specimen BU4–S3 with $e_c = 0.93$, and $N_{\gamma SA=3\%} = 1.2$ and $N_{\gamma_{SA}=3.75\%} = 13.3$ was smaller than Specimen BU4–S2 ($e_c = 0.96$, $N_{\gamma_{SA}=3\%} = 4.7$ and $N_{\gamma_{SA}=3.75\%} = 13.8$). Such an observation stems in part from the selected cyclic failure criteria; Specimen BU4 exhibited a consistent increase in cyclic resistance when considering $\gamma_{SA} = 5\%$ as the cyclic failure criterion (Table 3). Similarly based on the number of cycles required to achieve a particular $r_{u,max}$, Specimen BU4 exhibited a consistent increase in cyclic resistance, where $N_{r_{u,max}=60\%}$ increased from 10.5 for S2 to 25.5 for S3. Conclusions drawn from the r_u-based cyclic resistance differ from those using strain-based cyclic failure criteria (e.g., $\gamma_{SA} = 3\%$ or 3.75%), as revealed by inspection of the first quarter cycle of loading in the stress paths and γ–N for S2 and S3; S3 produced greater γ and r_u compared to S2 which resulted in lower N to reach $\gamma_{SA} = 3\%$ or 3.75%, whereas the overall cyclic resistance of the specimen improved due to the four shearing stages.

The difference in cyclic response of Specimens BU4 and BU2 was compared in terms of symmetry of γ accumulation in the early stages of loading (Table 3; considering that $\gamma_{max} < 5.9\%$). Although Specimen BU4 developed symmetric shear strains during S1 and S2, it exhibited a reduction in cyclic resistance for S3 ($N_{\gamma_{SA}=3.75\%}$). On the contrary Specimen BU2 exhibited consistent increase in cyclic resistance ($N_{\gamma_{SA}=3.75\%}$), despite the development of biased *CSR*-γ hysteresis in S2 and S3. It is inferred that symmetric strain accumulation with comparable γ_{max} in earlier shearing stages cannot guarantee a consistent trend in shearing response in subsequent loading phases, in contrast with the observations reported by Sanin [28] and Wijewickreme et al. [26].

The observed differences in cyclic response of intact specimens subjected to staged loading suggested that the inherent variability in soil properties from specimen to specimen may serve to obscure the governing physical mechanisms; reconstituted specimens can therefore serve to address the effect of specimen variability. Reconstituted Specimen BR1-S1 was subjected to $CSR = 0.20$ and terminated after $N = 33$ corresponding to $\gamma_{max} = 10.6\%$, followed by BR1-S2, BR1-S3, and BR1-S4 (Fig. 6). Fig. 6a, e, 6j, and 6 m demonstrate an increasing trend in cyclic resistance with increased loading stages at constant *CSR* with $N_{\gamma_{SA}=3.75\%} = 18$, 44, and >51 for BR1-S1, BR1-S2, and BR1-S3, respectively. Specimen BR1-S4 was subjected to a larger $CSR = 0.25$ but did not achieve $\gamma_{max} = 3.75\%$ after $N = 720$. The evolution of cyclic resistance in Specimen BR1 is similar to the intact Specimens BU1, BU2, and BU3, illustrating progressive increases in cyclic resistance for

Table 2
Summary of investigated parameters and corresponding metrics on cyclic resistance of soil.

Investigated Parameter	Corresponding Metric
Constant-volume, Staged, Stress-controlled Test	
Plasticity Index, *PI*	Site B, $PI = 14$ Site D, $PI = 26$
Overconsolidation Ratio, *OCR*	Site B, $OCR = 1.4$ to 2.0 Site D, $OCR = 1.6$ to 2.2
Natural Soil Fabric	Intact and reconstituted specimens tested from Sites B and D
Density	Post-cyclic volumetric strain Post-cyclic undrained shear strength
Shear Strain Failure Criterion	$N_{\gamma_{SA}=3\%}$, $N_{\gamma_{SA}=3.75\%}$, and $N_{\gamma_{SA}=5\%}$,
Excess Pore Pressure Response	$N_{r_{u,max}=60\%}$, and $N_{r_{u,max}=85\%}$ $r_{u,max}$ versus γ_{max} for $N = 1$, 10, and 20.
Constant-volume, Staged, Strain-controlled Test	
Overconsolidation Ratio, *OCR*	Reconstituted specimen from Site D with $OCR = 1$ and 2.
Soil Fabric	Shear wave velocity, V_s
Density	Post-cyclic volumetric strain Post-cyclic undrained shear strength
Excess Pore Pressure Response	$r_{u,max}$ versus γ_{max} for $N = 1$ to 30
Amplitude of Previously Experienced Shear Strain	$\gamma_{max} = 0.04$, 0.08, 0.5, 1, and 3%

Table 3
Test parameters and summary of results from constant-volume, staged, stress–controlled DSS tests on Site B specimens.

Test ID	Shear Stage No.	*OCR*	Vertical Effective Consolidation Stress σ'_{vc} (kPa)	Cyclic Stress Ratio *CSR*	Void Ratio e_c	Maximum Positive Shear Strain γ^{+}_{max} (%)	Absolute Maximum Negative Shear Strain γ^{-}_{max} (%)	N_{max}	Maximum excess pore pressure ratio $r_{u,max}$ (%)	Post-cyclic volumetric strain ε_{vpc} (%)	$N_{\gamma SA=3\%}$	$N_{\gamma SA=3.75\%}$	$N_{\gamma SA=5\%}$	$N_{ru,max = 60\%}$	$N_{ru,max = 85\%}$
BU1 (B-14)[a]	S1	1.5	160	0.26	0.89	8.5	8.1	25.5	92	2.5	6.8	10.7	15.8	6.0	16.0
	S2			0.26	0.84	3.9	5.3	114.5	81	1.2	23.8	47.8	102.8	22.0	114.5[c]
	S3			0.26	0.82	2.1	3.0	136.6	55	0.5	130.8	136.6[b]	136.6[b]	137.0[c]	137.0
BU2 (B-13)	S1	1.9	50	0.33	1.50	5.7	5.0	36.7	92	1.6	17.8	24.8	33.3	6.0	23.1
	S2			0.33	1.46	5.2	2.6	112.2	85	1.2	25.3	54.3	104.3	14.0	112.2[b]
	S3			0.33	1.43	3.2	2.5	247.4	75	NA[d]	196.3	247.7[a]	247.7[b]	53.0	247.7[c]
BU3 (B-13)	S1	2.0	48	0.31	1.47	5.2	4.6	86.7	88	1.8	49.3	65.3	84.3	17.5	70.1
	S2			0.31	1.42	5.1	1.9	213.0	81	1.2	51.3	113.3	205.3	34.0	213.0[c]
	S3			0.31	1.40	2.7	1.7	351.6	66	NA[d]	351.6	351.6[a]	351.6[b]	351.6[c]	351.6[c]
BU4 (B-14)	S1	1.5	160	0.27	0.99	5.9	5.6	8.1	80	2.0	2.3	13.77 13.29 226*	6.3	3.5	8.1[c]
	S2			0.28	0.96	5.1	5.3	30.6	79	1.6	4.7	13.8	27.8	10.5	30.6[c]
	S3			0.28	0.93	5.0	3.1	74.1	73	1.1	1.2	13.3	74.1	25.5	74.1[c]
	S4			0.28	0.91	3.0	3.0	225.9	61	NA[d]	205.3	225.9[b]	225.9[b]	202.5	225.9[c]
BR1 (B-14)	S1	1.5	160	0.20	0.81	10.6	9.8	33.0	91	4.0	18.2	20.3	23.3	12.0	25.0
	S2			0.20	0.73	6.1	4.1	100.6	86	2.0	44.3	59.3	81.3	20.0	93.0
	S3			0.20	0.70	1.8	1.5	51.2	46	0.5	51.0	51.2[b]	51.2[b]	51.2[c]	51.2[c]
	S4			0.25	0.69	3.3	2.6	720.0	70	0.9	579.3	720.0[b]	720.0[b]	370.0	720.0[c]
BR2 (B-14)	S1	1.5	160	0.22	0.84	13.1	13.8	22.5	88	4.0	7.7	9.7	12.7	5.5	14.0
	S2			0.22	0.76	6.2	12.3	90.6	86	2.4	16.8	25.8	40.8	11.5	73.5
	S3			0.22	0.72	4.8	6.2	200.0	86	NA[d]	3.8	14.8	86.8	11.5	179.1

[a] Borehole Designation.
[b] These specimens did not reach the target shear strain amplitude (i.e., $\gamma_{SA} = 3.75\%$) for the stated number of loading cycles.
[c] These specimens did not reach the target maximum excess pore pressure ratio (i.e., $r_{u,max} = 60\%$) for the stated number of loading cycles.
[d] NA = Not available.

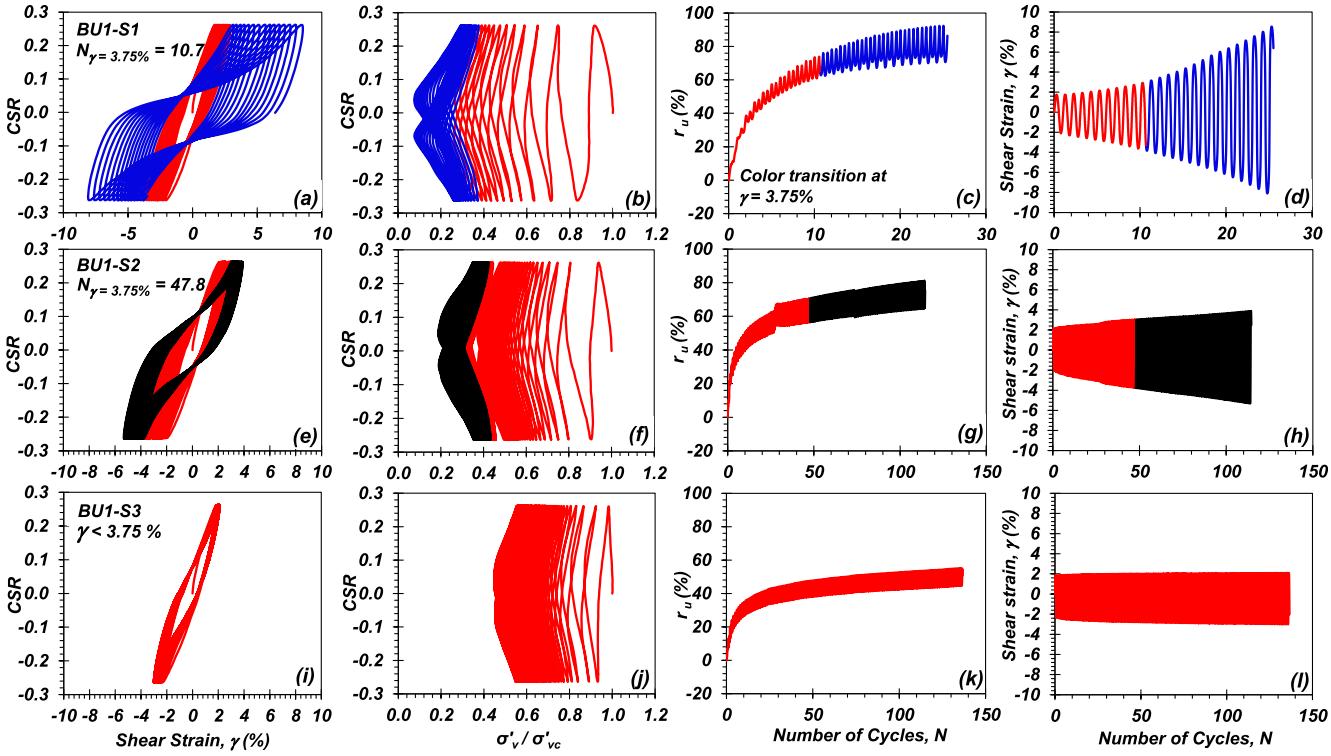

Fig. 4. Cyclic response of intact specimen BU1 subjected to staged, stress-controlled cyclic DSS test indicating cyclic shear stress-shear strain hysteresis (a, e, i), effective stress paths (b, f, j), generation of excess pore pressure with *N* (c, g, k), and accumulation of shear strain with *N* (d, h, l): (a–d) Stage 1, (e–h) Stage 2, and (i–l) Stage 3.

subsequent loading events where the reduction of void ratio as a result of post-cyclic reconsolidation and possible improvements in lateral stress represent the primary cause of the increased cyclic resistance. In contrast to Specimen BR1, Specimen BR2 exhibited degradation in cyclic resistance when assessed using strain failure criteria; however, it showed improvement in cyclic resistance evaluated based on excess pore pressure generation. The observed contrast could be attributed to the large asymmetric accumulation of shear strain in BR2-S2 ($\gamma_{max} = 12.3\%$) which likely resulted in a spatially-variable distribution of density and development of local instabilities within the specimen [27,60]. The *CSRs* applied to the denser reconstituted specimens were considerably smaller than those of the intact specimens due to the weakness of their younger, less-developed soil fabric. Likewise, the post-cyclic volumetric strains were larger, consistent with observations by others [34,61–65].

In summary, the amplitude of maximum shear strain, γ_{max}, which can adversely affect the soil fabric and result in the degradation of cyclic resistance (γ-based), may be different for intact ($\gamma_{max} = 5.9\%$; BU4) and reconstituted specimens ($\gamma_{max} = 13\%$; BR2). However, both intact and reconstituted specimens exhibited consistent increase in the cyclic resistance assessed based on r_u response ($N_{r_{u,max}}$). This observation is not well-aligned with the results reported by Soysa and Wijewickreme [25] and Wijewickreme et al. [26] for normally consolidated nonplastic reconstituted Fraser River Silt, which exhibited a consistent trend in evolution of cyclic resistance assessed based on shear strain failure criteria and excess pore pressure response. The implied inconsistency with the results of prior studies [25,26] is likely attributable to differences in the material properties of the soils (e.g., *PI*, *OCR*, *FC*, and soil fabric). Further research to elucidate the role of γ_{max} on the cyclic response of silts is warranted.

3.2. Constant-volume stress-controlled tests on high plasticity (Site D) silts

Table 4 summarizes the cyclic response of intact (i.e., DU1, DU2, DU3, and DU4) and reconstituted specimens (i.e., DR1, DR2, and DR3) derived from Site D. Fig. 7a–d presents the progressive increase in cyclic resistance of Specimen DU1 subjected to $CSR = 0.31$ for the three stages of cyclic loading, where $N_{\gamma_{SA}=3.75\%} = 6.8$, 42.8, and >255 for S1, S2, and S3, respectively. Fig. 7e–h illustrate the two cyclic loading stages of Specimen DU2 subjected to constant $CSR = 0.36$. The first quarter cycle of loading of S1 achieved $\gamma = 2.9\%$ with continued loading to $\gamma_{max} = 18.5\%$ and corresponding to $N = 19.2$ (Fig. 7e). However, in the following stage Specimen DU2 produced $\gamma = 9.1\%$ during first quarter cycle of loading, resulting in the significantly lower $N_{\gamma_{SA}=3.75\%}$ as compared to S1. The observed reduction in cyclic resistance occurred despite the symmetric accumulation of γ and considerable densification following S1 (i.e., $\varepsilon_{vpc} = 4.9\%$; Table 3). Destruction of the soil fabric, reduction in lateral stress, and possible shear induced anisotropy due to the large $\gamma_{max} = 18.5\%$ are the primary reasons for the degradation in cyclic resistance [27].

The constant-volume, staged, cyclic test on Specimen DU3 was specifically conducted to investigate the effect of γ_{max} on cyclic resistance for the subsequent loading events. Specimen DU3-S1 was subjected to $CSR = 0.21$ which developed $\gamma_{max} = 1.2\%$ after $N = 304$, whereas in the second stage, DU3 was sheared under the same *CSR* as Specimen DU2 ($CSR = 0.36$), which generated $\gamma_{max} = 24\%$ corresponding to $N = 26.2$. Although Specimens DU2-S2 and DU3-S2 have comparable void ratios (Table 4), DU3-S2 exhibited greater cyclic resistance ($N_{\gamma_{SA}=3.75\%} = 6.3$) than DU2-S2 ($N_{\gamma_{SA}=3.75\%} = 0.2$) for the same *CSR*, and exhibited a dilative tendency, in contrast to the contractive tendency of DU2-S2, for their first quarter cycles (Fig. 7f and j). The larger amplitude of γ_{max} for DU2-S1 ($\gamma_{max} = 18.5\%$) caused detrimental effects to soil fabric and resulted in a lower cyclic resistance [28] relative to DU3-S1 ($\gamma_{max} = 1.2\%$).

The evolution of cyclic resistance in the reconstituted NC specimens from Site D (DR1, DR2, and DR3) with $\sigma'_{vc} = 200$ kPa was investigated using staged loadings with constant *CSR* (with the exception of DR2-S3; Table 4). Fig. 8 presents the cyclic response of Specimen DR1, with γ_{max}

Table 4
Test parameters and summary of test results of constant-volume, staged, stress–controlled test for Site D specimens.

Test ID	Shear Stage No.	*OCR*	Vertical Effective Consolidation Stress σ'_{vc} (kPa)	Cyclic Stress Ratio, *CSR*	Void Ratio, e_c	Maximum Positive Shear Strain, γ^{+}_{max} (%)	Absolute Maximum Negative Shear Strain, γ^{-}_{max} (%)	N_{max}	Maximum excess pore pressure ratio, $r_{u,max}$ (%)	Post-cyclic volumetric strain, ε_{vpc} (%)	$N_{\gamma SA=3\%}$	$N_{\gamma SA=3.75\%}$	$N_{\gamma SA=5\%}$	$N_{ru,max = 60\%}$	$N_{ru,max = 85\%}$
DU1	S1	2.1	118	0.31	1.89	3.1	5.0	16.4	57	1.4	2.8	6.8	15.8	16.4[a]	16.4[a]
	S2			0.31	1.85	2.3	4.3	155.6	51	1.0	4.5	42.8	155.5[1]	155.5[2]	155.5[2]
	S3			0.31	1.82	1.8	3.4	255.0	39	0.5	7.8	255.0[1]	255.0[1]	255.0[2]	255.0[2]
DU2	S1	1.9	118	0.36	2.13	18.5	17.2	19.2	78	4.9	0.8	2.2	4.7	6.0	19.2[1]
	S2			0.36	1.98	12.3	5.7	12.8	62	NA	0.1	0.2	0.2	11.0	12.8[2]
DU3	S1	1.8	118	0.21	2.11	1.2	0.8	304.0	41	0.7	304.0[1]	304.0[1]	304.0[1]	304.0[2]	304.0[2]
	S2			0.36	2.09	24.0	18.5	26.2	87	NA	4.3	6.3	10.4	9.6	23.6
DU4	S1	1.9	118	0.25	2.02	2.3	1.2	232.5	59	3.0	232.5[1]	232.5[1]	232.5[1]	232.5[2]	232.5[2]
	S2			0.37	1.93	4.3	8.9	101.6	73	NA	3.8	12.8	45.8	60.6	101.6[2]
DR1	S1	1.0	200	0.25	1.21	6.9	8.0	10.5	78	3.3	3.7	4.7	6.7	6.0	10.5[2]
	S2			0.25	1.13	6.2	7.7	62.4	82	2.9	12.7	23.8	40.8	22.5	62.4[2]
	S3			0.25	1.07	2.2	3.5	393.7	72	1.5	6.8	109.7	393.7[1]	115.0	393.7[2]
DR2	S1	1.0	200	0.20	1.24	7.0	8.3	43.3	86	3.8	27.0	31.0	35.8	21.5	42.0
	S2			0.20	1.15	2.1	2.4	295.0	64	1.1	295.0[1]	295.0[1]	295.0[1]	199.0	295.0[2]
	S3			0.30	1.13	7.5	8.3	107.5	78	2.5	21.0	50.0	77.8	54.5	107.4[2]
DR3	S1	1.0	200	0.30	1.25	7.9	7.5	2.5	63	2.6	0.3	0.7	1.7	2.5	2.5[2]
	S2			0.30	1.19	6.5	8.3	9.5	71	2.4	0.3	1.8	4.7	5.5	9.5[2]
	S3			0.30	1.14	5.6	7.9	37.4	75	2.0	0.7	2.8	14.8	15.5	37.4[2]

3 NA = Not available.
[1] These specimens did not reach the target shear strain amplitude (e.g., $\gamma_{SA} = 3\%$) for the stated number of loading cycles.
[2] These specimens did not reach the target maximum excess pore pressure ratio (i.e., $r_{u,max} = 60\%$) for the stated number of loading cycles.

Table 5
Summary of specimen properties and loading type for staged, strain-controlled cyclic tests.

Test No.	Loading Type	Void Ratio, e_c	Vertical Effective Consolidation Stress, σ'_{vc} (kPa)	*OCR*	Shear Wave Velocity, V_s at σ'_{vc} (m/s)	Shear Wave Velocity at σ'_{vc} = 150 kPa, $V_{s,150}$ (m/s)
NC-S	S	1.07	200	1.0	NA	NA
NC-L	L	1.10	200	1.0	154	NA
OC-S	S	1.12	100	2.0	151	138
OC-L	L	1.11	100	2.0	149	135

[1] NA = Not available.

= 8% and corresponding to $N = 10.5$ for the first loading stage. Specimen DR1 exhibited improvement in cyclic resistance following each stage with $N_{\gamma_{SA}=3.75\%} = 4.7$, $N_{\gamma_{SA}=3.75\%} = 23.8$, and $N_{\gamma_{SA}=3.75\%} = 109.7$ for S1, S2 and S3, respectively, due to the sequential reduction in void ratio and possible increase in lateral stress. The variation in cyclic resistance of NC Specimens DR1, DR2, and DR3 can be interpreted in terms of the pseudo-overconsolidation, OCR_e concept [66,67] as a result of sequential reduction in void ratio under identical σ'_{vc}. The OCR_e was calculated for NC specimens by assuming that the compression and recompression indices (i.e., C_c and C_r) remain constant between loading stages. For example, the apparent OCR_e for NC Specimen DR1 after two reconsolidation stages is interpreted equal to 2.7 (Table S1). Similar increases in cyclic resistance and corresponding OCR_e were observed for Specimens DR2 and DR3 as summarized in Tables 4 and S1, respectively. The evidence for the detrimental effect of large shear strains on the subsequent cyclic response is also provided in Table 4. For example, under constant $CSR = 0.3$, DR2-S3 and DR3-S3 with $e_c = 1.13$ and 1.14, exhibited $N_{\gamma_{SA}=3.75\%} = 50$ and 2.8 with developed $\gamma_{max} = 2.4$ and 8.3%, respectively, during the second stage.

3.3. Synthesis of observations from stress-controlled tests

Fig. 9 presents the variation of *CSR* with $N_{\gamma_{SA}=3\%}$ and $N_{\gamma_{SA}=3.75\%}$ for intact (Fig. 9a and b) and reconstituted (Fig. 9c and d) specimens from Sites B and D to illustrate the role of the selected cyclic failure criterion on the interpreted effect of pre-straining. For example, Specimens DR1 and DR3 exhibited progressive increases in $N_{\gamma_{SA}=3.75\%}$ (Fig. 9d) compared to the inconsistent changes in cyclic resistance using $N_{\gamma_{SA}=3\%}$ (Fig. 9c), since for the latter stages of loading the dilative tendency decreases the rate of shear strain accumulation per number of cycles as a result of post-cyclic densification and pseudo-overconsolidation, where the required number of cycles to reach some predefined γ is highly dependent on amplitude of γ in first cycle of loading. Therefore, cyclic resistance is sensitive to the shear strain failure criterion selected [27].

Excess pore pressure generation potential can serve to clarify some of the inconsistent observations in cyclic response assessed based on failure strain criteria. Fig. 10 presents the variation of $r_{u,max}$ with γ_{max} as a function of N and indicates that $r_{u,max}$ is more sensitive to γ_{max} than N as observed by Dahl et al. [68] and Jana and Stuedlein [34]. Reductions in $r_{u,max}$ for a given N and γ_{max} as the number of loading stages increases may be interpreted as an improvement in cyclic resistance. For $\gamma_{max} =$ 3.6% and $N = 10$, the intact specimens from Site B exhibited $r_{u,max} =$ 72% in Stage 1 and reduced to 60% and 48% in Stages 2 and 3, respectively. The observed reduction in pore pressure generation indicates improvement in cyclic resistance due to increases in dilatancy resulting from post-cyclic densification, apparent pseudo-overconsolidation, and the presumable increase in lateral stress.

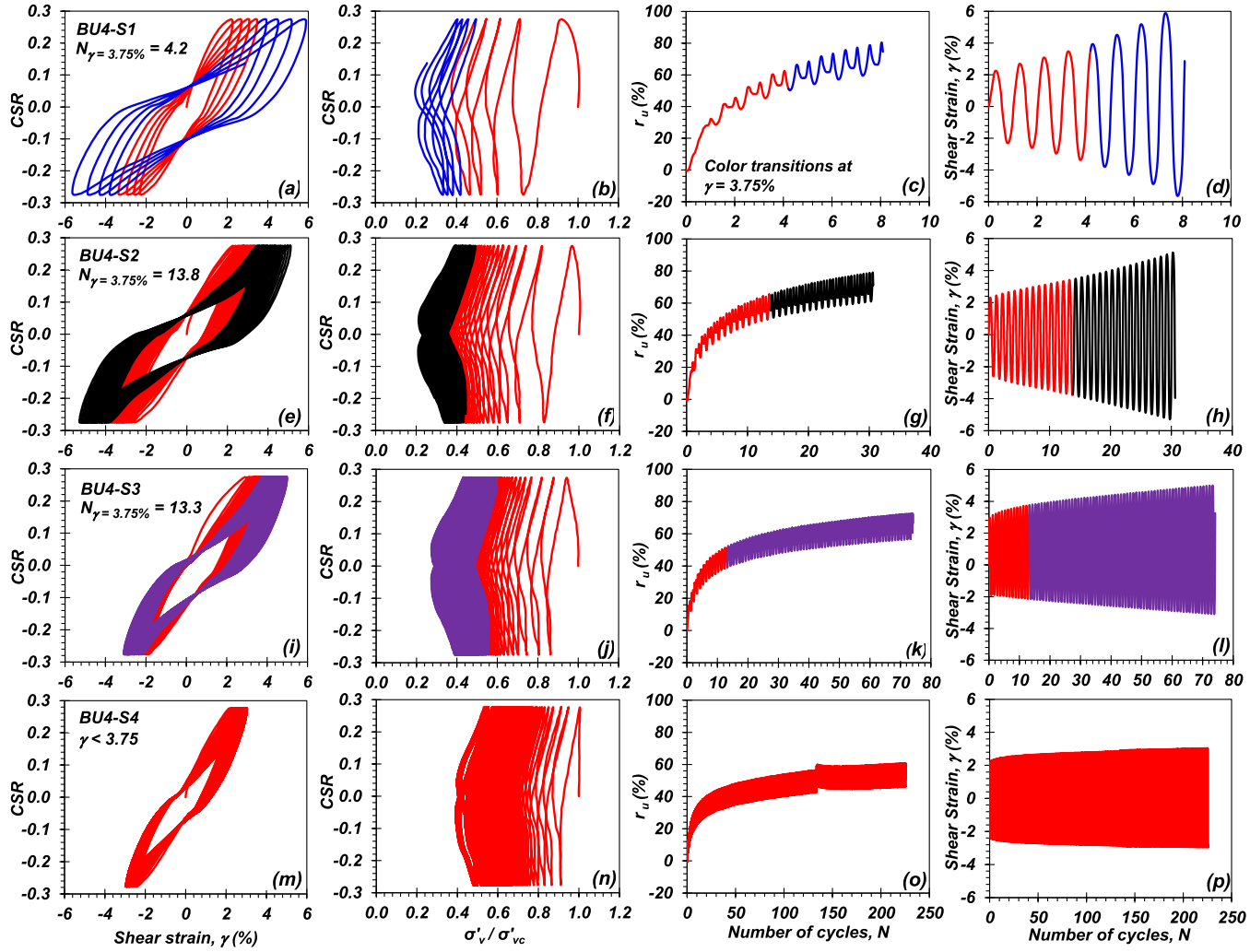

Fig. 5. Cyclic response of intact specimen BU4 subjected to staged, stress-controlled cyclic DSS test indicating cyclic shear stress-shear strain hysteresis (a, e, i, and m), effective stress path (b, f, j, and n), generation of excess pore pressure with *N* (c, g, k, and o), and accumulation of shear strain with *N* (d, h, l, and p): (a–d) Stage 1, (e–h) Stage 2, (i–l) Stage 3, and (m–p) Stage 4.

The cyclic response of intact Specimens BU3 and DU1, subjected to similar $CSR = 0.31$, exhibited consistent increases in cyclic resistance (based on $N_{\gamma_{SA}=3.75\%}$ and $N_{r_{u,max}}$) for the subsequent stages (BU3: Table 3 and Fig. S9; DU1: Table 4 and Fig. 7a–d). Specimen BU3 ($PI = 14$, $OCR = 2$, $e_c = 1.47$) exhibited greater cyclic resistance than Specimen DU1 ($PI = 26$, $OCR = 1.8$, $e_c = 1.89$) in terms of $N_{\gamma_{SA}=3.75\%}$ due to its greater density and *OCR*. However, Specimen BU3 exhibited smaller cyclic resistance than Specimen DU1 in terms of $N_{r_{u,max}}$ due to its lower plasticity (Table 4; Fig. S11). Similarly, the comparison of the cyclic response of reconstituted Specimens BR1 and DR2 subjected to $CSR = 0.20$ indicated a consistent increase in cyclic resistance in the subsequent stages (BR1: Table 3 and Fig. 6; DR2: Table 4 and Fig. S10). Although Specimen DR2 ($PI = 26$, $OCR = 1$, $e_c = 1.24$) has lower *OCR* and density compared to Specimen BR1 ($PI = 14$, $OCR = 1.4$, $e_c = 0.81$), it exhibited higher cyclic resistance (based on $N_{\gamma_{SA}=3.75\%}$ and $N_{r_{u,max}}$) because of its higher plasticity. In general, intact and reconstituted specimens subjected to at least two shearing-reconsolidation stages exhibited overall increases in cyclic resistance. However, intact specimens of Site B (i.e., BU1 and BU4) experienced smaller γ_{max} and reductions in *e* compared to their reconstituted counterparts with similar σ'_{vc} and *OCR*, and gained greater cyclic resistance in terms of $N_{\gamma = 3.75}$. The differences noted between the various intact and reconstituted specimens indicate that the effect of various contributing factors (i.e., natural soil fabric, *PI*, *OCR*, and density) on the cyclic resistance of plastic soils is difficult to isolate.

The use of a strain-based cyclic failure criterion is convenient for the assessment of cyclic resistance for use in the simplified method (e.g. Ref. [69]) of cyclic softening assessments; however, there is no fundamental basis for the selection of an arbitrary strain amplitude [70]. The results of this investigation clearly show how the selection of a strain-based failure criterion may impact the assessment of cyclic resistance of soil subjected to repeated cyclic loading, especially as the specimen densifies following multiple loadings or generates the inevitable asymmetrical *CSR*-γ hysteresis [27]. The alternative r_u-based interpretation may serve to improve the assessment of repeated loading on the cyclic resistance of plastic soils.

3.4. Constant-volume strain-controlled tests for Site D reconstituted specimens

In this testing procedure NC and OC Site D specimens were subjected to the small and large loading protocols designated S and L, respectively, as illustrated in Fig. 3e and f. Table 5 summarizes the properties of test specimens and loading program. To further understand the effect of overconsolidation on soil fabric, the shear wave velocity for Specimens OC-S and OC-L were measured at different loading steps before reaching the preconsolidation pressure of 200 kPa. For example, the measured V_s at $\sigma'_{vc} = 150$ kPa during the loading path to $OCR = 1$ is reported in

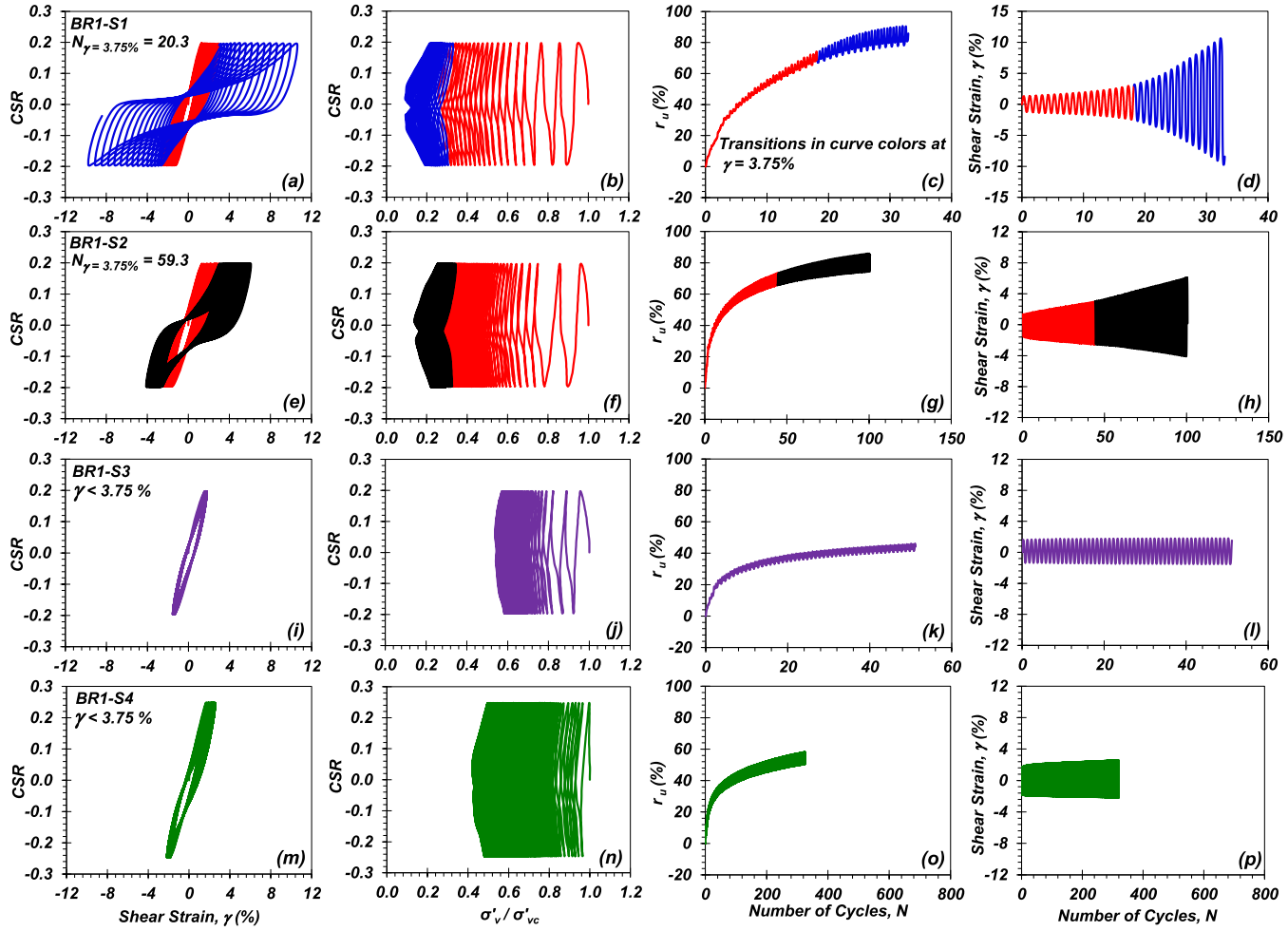

Fig. 6. Cyclic response of reconstituted specimen BR1 subjected to staged, stress-controlled cyclic DSS test indicating cyclic shear stress-shear strain hysteresis (a, e, i, and m), effective stress path (b, f, j, and n), generation of excess pore pressure with N (c, g, k, and o), and accumulation of shear strain with N (d, h, l, and p): (a–d) Stage 1, (e–h) Stage 2, (i–l) Stage 3, and (m–p) Stage 4.

Table 5. Specimens OC-S and OC-L exhibit higher V_s at $\sigma'_{vc} = 100$ kPa (i.e., $OCR = 2$) than when they are subjected to $\sigma'_{vc} = 150$ kPa due to the dominance of stress history on soil fabric and V_s overshadowing the effect of effective stress amplitude.

3.4.1. Typical excess pore pressure response of NC and OC specimens

Fig. 11 presents the variation of r_u with N for NC and OC specimens subjected to S and L loadings. The NC and OC specimens exhibited a net reduction in excess pore pressure generation as the number of cyclic loading and reconsolidation stages increases. For example, all specimens exhibited lower r_u in Stage 12 (i.e., S12, Fig. 11c, f, 11j, and 11l) compared to Stage 4 (Fig. 11a, d, 11g, and 11j) at a constant shear strain amplitude, which is attributed to the dilative tendency resulting from pseudo-overconsolidation and post-cyclic densification. Specimen NC-L exhibited positive r_u at $N = 1$ of S4 (Fig. 11d), whereas S12 produced negative (i.e., dilative) r_u (Fig. 11f) due to the increased density and OCR_e (i.e., from 1.1 at S4 to 1.7 at S12; Table S1). OC specimens developed significant negative r_u at $N = 1$ in S4 (Fig. 11g and j) due to the stress history of the specimen, since the insignificant r_u generated prior to S4 resulted in negligible densification ($\varepsilon_{vpc} < 0.01\%$) as described below.

3.4.2. Effect of small and large shaking on cyclic resistance

Fig. 12 presents the staged, cyclic response of OC and NC specimens subjected to small (Fig. 12a) and large (Fig. 12b) shakings. The variation in residual excess pore pressure ratio, $r_{u,r}$, for NC and OC specimens subjected to S loading indicated that $r_{u,r}$ progressively decreased between the first and last stages for both smaller (S1, 2, 3, 5, 6, 7, 9, 10, and 11) and larger shear strain amplitudes (S4, 8, and 12). For example, Specimen OC-S subjected to constant $\gamma = 1\%$ in S4, 8, and 12 exhibited reduction in $r_{u,r}$ from 8.5% at S4 to 5.3% and 3.9% in S8 and S12, respectively. The 54% reduction in $r_{u,r}$ from S4 to S12 is interpreted as an improvement in cyclic resistance in spite of the near-constant void ratio and minor increase in V_s (i.e., 0.1%; Fig. 12f) over these loading stages. These trends may also be observed for stages characterized with smaller shear strain amplitudes. Although the small shaking did not result in significant changes in density, a stronger soil fabric was developed as indicated by the change in V_s, inferred to have developed through the removal of local instabilities, increase in lateral stress, and rearrangement of soil particles [7,20], consistent with the effect of pre-shaking on a young, reconstituted silty sand reported by El-Sekelly et al. [6] and NC Drammen Clay ($PI = 27$) reported by Andersen et al. [22].

Fig. 12d illustrates the effect of large shaking (i.e., L loading) on the generation of $r_{u,r}$ in NC and OC specimens. Specimen NC-L exhibited a reduction in $r_{u,r}$ for stages with smaller (S1, 2, 3, 5, 6, 7, 9, 10, and 11) and larger amplitudes of shear strain similar to Specimens OC-S and NC-S. For instance, under a constant $\gamma = 0.5\%$ Specimen NC-L produced $r_{u,r} = 9.75\%$ at the end of S3, which reduced to 3.75% at the end of S11. The 61% reduction in $r_{u,r}$ from S3 to S11 was associated with 6.4% reduction in e_c (Fig. 12e), the increase in OCR_e from 1.0 to 1.7 (Table S1), and 4%

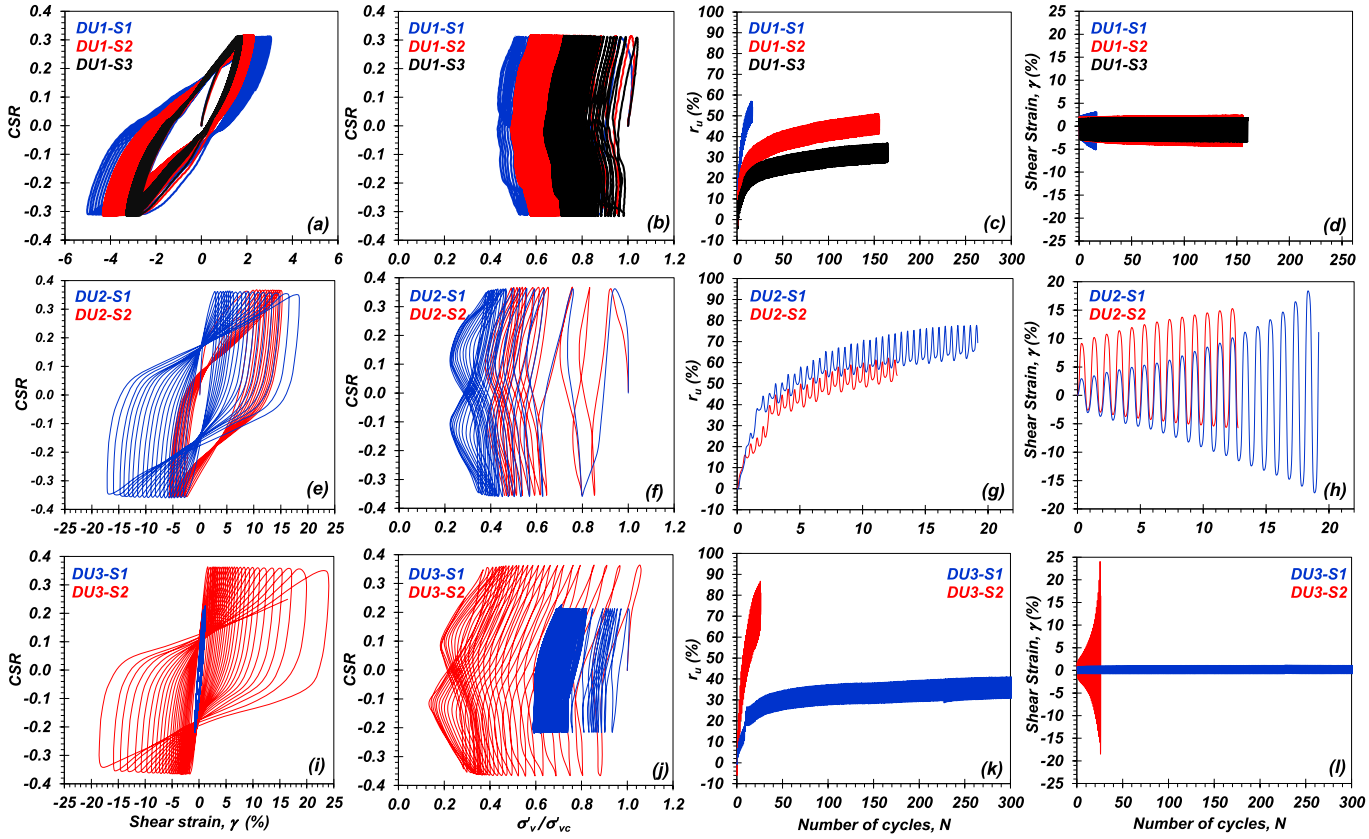

Fig. 7. Cyclic response of intact specimens DU1, DU2, and DU3 subjected to staged, stress-controlled cyclic DSS tests indicating shear stress-shear strain hysteresis (a, e, and i), effective stress paths (b, f, and j), generation of excess pore pressure with N (c, g, and k), and accumulation of shear strain with N (d, h, and l): (a–d) specimen DU1, (e–h) specimen DU2, and (i–l) specimen DU3.

increase in V_s (Fig. 12f). The trend in the reduction of $r_{u,r}$ is similar for S4 and S8 associated with larger shear strain amplitudes. Although the S4 loading with $\gamma = 3\%$ may have destroyed the soil fabric and partially or totally removed the beneficial effect of prior low amplitude cyclic shear strains (i.e., S1 through S3), post-cyclic densification and possible increase in lateral stress produced a more dilative response.

Specimen OC-L exhibited significantly different cyclic behavior than that of NC-L. Fig. 12d shows that subjecting the specimen to S4 loading with large shear strain amplitude ($\gamma = 3\%$) resulted in a significant generation of $r_{u,r}$ for the following small-strain loading stage: the constant $\gamma = 0.04\%$ generated zero $r_{u,r}$ at S1 compared to $r_{u,r} = 8\%$ as a result of S5. The reduction in V_s from 149 m/s at S1 to 141 m/s at S5 (Fig. 12f) indicates some degree of fabric destruction, removal of the beneficial effects of low amplitude cyclic straining, presumably a reduction in lateral stress, and confirms the observed changes in excess pore pressure response. The observed reduction in resistance occurred despite the reduction in void ratio from S1 to S4 (i.e., from $e_c = 1.11$ to 1.09; Fig. 12e). A similar trend is noted when comparing $r_{u,r}$ for S7 and S6 with S3 and S2, respectively. These observations generally agree with the findings developed for reconstituted, overconsolidated silt ($PI = 0$ and $PI = 6$) reported by Price et al. [27], and the results of triaxial and simple shear tests conducted by Andersen et al. [22] on overconsolidated intact Drammen clay ($PI = 27$) for application to offshore geotechnics. Specimen OC-L was able to recover some of its original cyclic resistance ($r_{u,r}$-based) following S8 (Fig. 12d). For example, the $r_{u,r}$ for Specimen OC-L was 6.7% (Fig. 12d) at the end of S11, which was smaller than that of S7 ($r_{u,r} = 7.9\%$), but still greater than that of S3 ($r_{u,r} = 1.9\%$); changes in the magnitude of $r_{u,r}$ were well-captured by the variation in the corresponding V_s (Fig. 12f).

In summary, NC-S and OC-S specimens subjected to small shaking exhibited consistent trends in the reduction of excess pore pressure generation during cyclic loading as the specimen experiences progressively greater cyclic-reconsolidation stages. However, during large shaking stress history plays a critical role in the reduction in cyclic resistance ($r_{u,r}$-based) following the first large strain amplitude stage, with the possibility of a substantial and detrimental change in the soil fabric. In the following stages during large shaking, Specimen OC-L recovered some of its resistance and followed a similar reduction in excess pore pressure generation as that of the NC-L specimen (Fig. 12f). Although Specimens NC-L and OC-L have experienced considerable reduction in e following large strain (Stage 4) loading, associated with significant excess pore pressure generation, V_s decreased notably. Furthermore, the variation in V_s with stage in Specimens OC-S, NC-L, and OC-L (Figs. 12f and S12) appears more sensitive to the changes in soil fabric than the variation in density.

3.5. Effect of strain history on monotonic undrained response

Following completion of the last cyclic loading stage in the stress and strain-controlled tests, selected specimens were re-centered in the DSS device and reconsolidated to σ'_{vc} followed by constant-volume, monotonic shearing at a strain rate of 5%/h. The primary objective was to investigate the evolution of undrained shear strength, $s_{u,DSS}$, due to multiple cyclic loading and reconsolidation events. The methodology is similar to the use of cone penetration tests (CPT) following physical model laboratory tests [21,71] to capture changes in soil strength subjected to prior seismic events. Fig. 13 presents the comparison of stress-strain responses and effective stress paths of specimens with and without cyclic loading history. Table 6 summarizes the results of tests on specimens from Site D that were previously subjected to staged,

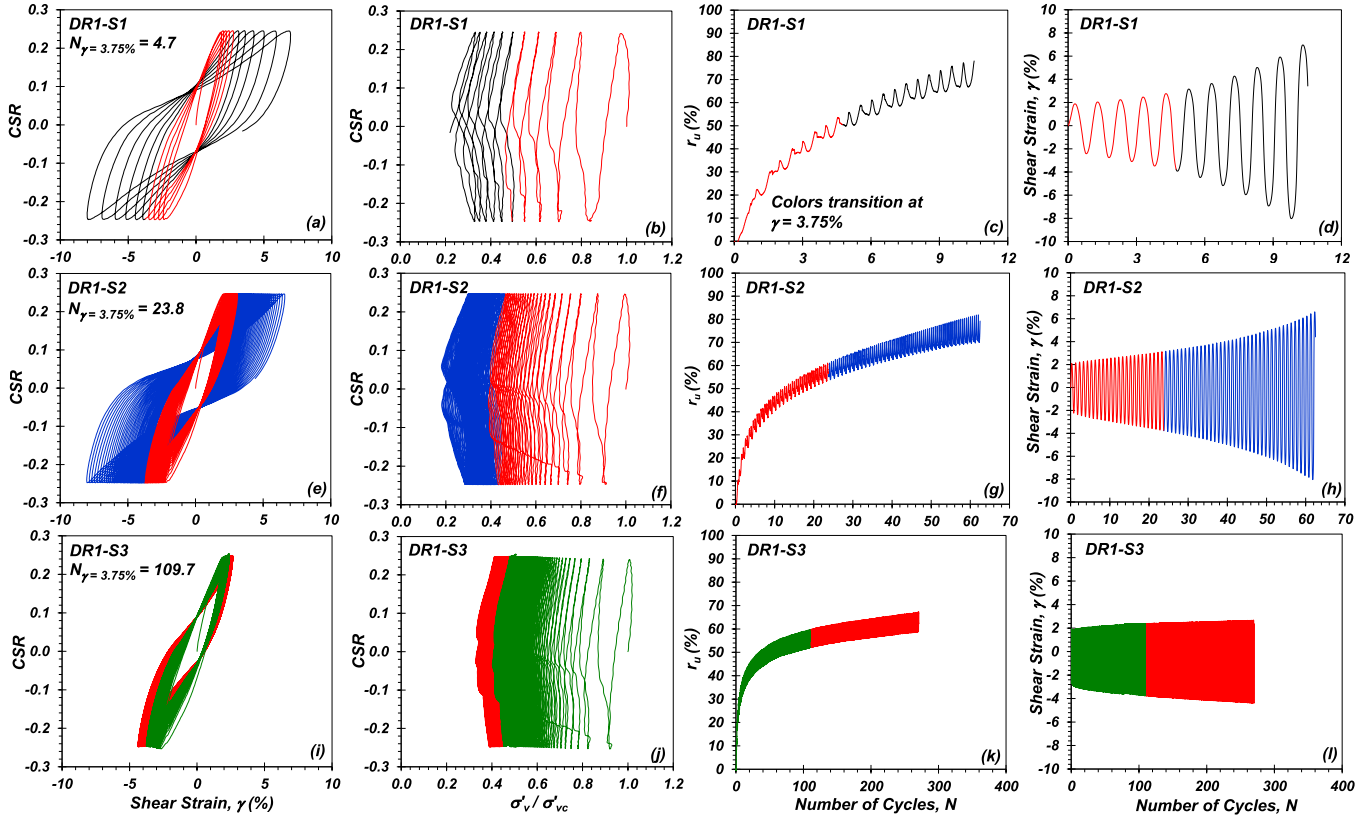

Fig. 8. Cyclic response of reconstituted specimen DR1 subjected to staged, stress-controlled cyclic DSS test indicating shear stress-shear strain hysteresis (a, e, and i), effective stress path (b, f, and j), generation of excess pore pressure with *N* (c, g, and k), and accumulation of shear strain with *N* (d, h, and l): (a–d) Stage 1, (e–h) Stage 2, and (i–l) Stage 3.

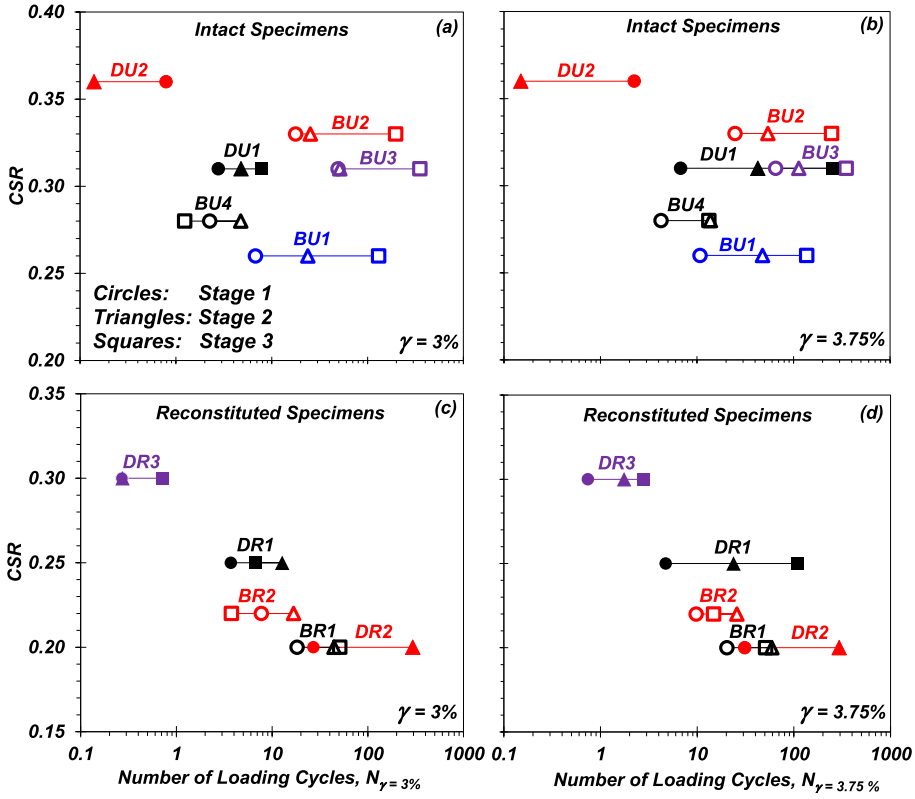

Fig. 9. Variation of *CSR* with *N* for: (a) γ_{SA} = 3% and (b) γ_{SA} = 3.75% for intact specimens, (c) γ_{SA} = 3% and (d) γ_{SA} = 3.75% for reconstituted specimens.

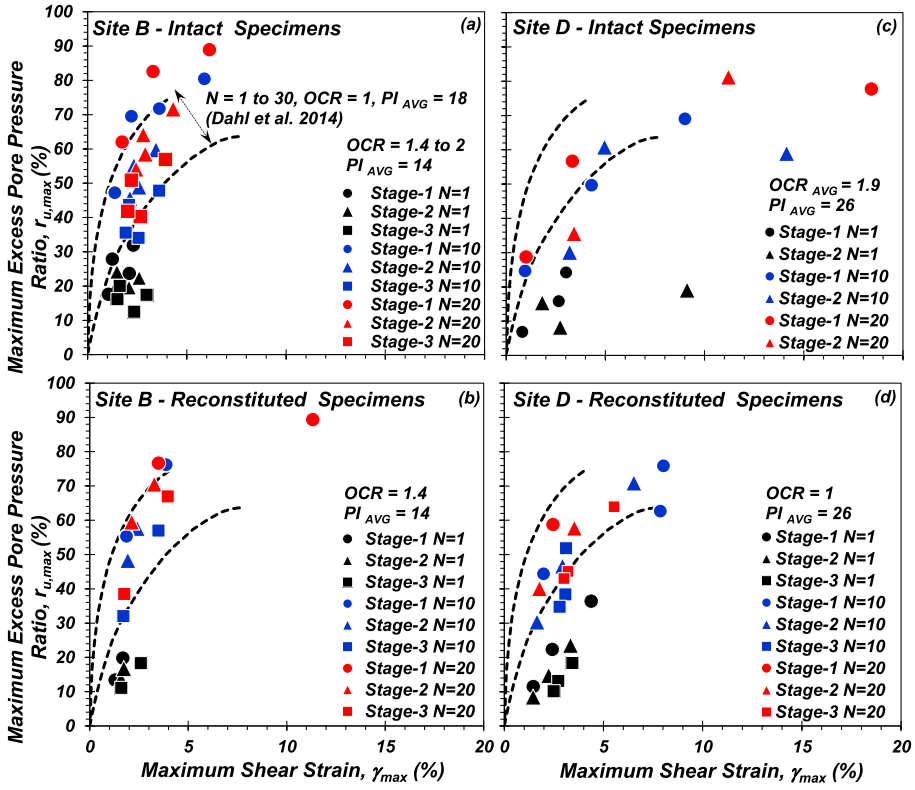

Fig. 10. Variation of maximum excess pore pressure ratio with number of cycles and maximum shear strain during staged, stress-controlled cyclic DSS tests: (a) intact specimens for Site B, (b) reconstituted specimens for Site B, (c) intact specimens for Site D, and (d) reconstituted specimens for Site D.

stress-controlled (i.e., DR1, DR2, and DR3; Table 4) or strain-controlled tests (i.e., NC-S, NC-L, OC-S, and OC-L; Table 5) along with the specimens without cyclic loading history (i.e., DR0, NC-0, and OC-0). The $s_{u,DSS}$ was selected equal to the shear stress corresponding $\gamma = 15\%$ [68] for those specimens exhibiting a strain hardening response.

The effective stress path of the virgin NC specimen, DR0, exhibited a contractive response (Fig. 13b), whereas the pre-strained and pseudo-overconsolidated NC specimens (i.e., DR1, DR2, and DR3) initially exhibited a dilative tendency to develop an $s_{u,DSS}$ that was significantly greater than the virgin specimen (Fig. 13a). The dilative tendency of the pre-strained specimens is attributed to the magnitude of the apparent OCR_e prior to monotonic shear (DR1: $OCR_e = 3.6$; DR2: $OCR_e = 3.6$; and DR3: $OCR_e = 3.4$; Table S1). Although Specimens DR1, DR2, and DR3 experienced comparable γ_{max} (8, 8.3, and 8.3%) during the prior cyclic loading (Table 3), Specimens DR1 and DR2 exhibited greater $s_{u,DSS}$ than DR3 due to their larger OCR_e. The $s_{u,DSS}$ of these three pre-strained specimens was approximately 120% greater than Specimen DR0 (Table 6), indicating that post-cyclic densification and accompanying increase in OCR_e and presumably an increase in lateral stress, are the primary reasons for the improvement in $s_{u,DSS}$. This observation is consistent with the reported increase in cone penetration resistance on reconstituted sand subjected to multiple loading events [21,71]. The $s_{u,DSS}$ of the pre-strained soil could be useful for the prediction of the cyclic resistance ratio, $CRR_{M=7.5}$ for $N = 30$, moment magnitude, $M_w = 7.5$ earthquake, and level ground within the simplified method proposed by Boulanger and Idriss [72] provided that the *CRR-N* curve can be quantified by a power law with exponent equal to 0.135. For an average undrained shear strength ratio, $s_{u,DSS}/\sigma'_{v0} = 0.65$ for the pre-strained NC specimens, $CRR_{M=7.5}$ would be 0.52, significantly higher than $CRR_{M=7.5} = 0.24$ corresponding to $s_{u,DSS}/\sigma'_{v0} = 0.3$ for virgin specimens.

Fig. 13c and d compares the τ_h/σ'_{vc} -γ and effective stress paths of virgin NC and OC specimens to that of the pre-strained specimens. The effective stress path of virgin Specimen NC-0 exhibited a highly-contractive response, whereas virgin Specimen OC-0 initially dilated followed by contraction (Fig. 13d). In contrast, the pre-strained specimens exhibited notable differences in volumetric tendency that varied with small or large shaking history. For example, Fig. 13d illustrates that the initial contractive tendency in Specimen NC-S was smaller than Specimen NC-0, whereas Specimen NC-L exhibited a slight, initial dilative response. These observations are consistent with the larger apparent OCR_e for Specimen NC-L ($OCR_e = 1.9$) than that of NC-S ($OCR_e = 1.2$). The $s_{u,DSS}$ of Specimens NC-S and NC-L increased by 30% and 64% relative to Specimen NC-0, respectively, due to the post-cyclic densification and accompanying increase in apparent OCR_e, which serve to improve the soil fabric (Fig. 12e and f).

Pre-strained Specimen OC-S ($e_c = 1.11$) exhibited a lower initial dilative tendency compared to virgin Specimen OC-0 ($e_c = 1.13$; Table 6). However, Specimen OC-L ($e_c = 1.06$; Table 6) exhibited an initial contractive response despite the lower void ratio. The reduction in the initial dilative tendencies of Specimens OC-S and OC-L relative to virgin Specimen OC-0 suggests that changes to the soil fabric inferred from V_s measurements (Fig. 12f) can only partially explain the observed initial monotonic shear behavior. However, the increased dilation at large shear strains can be attributed to the significantly higher density in Specimen OC-L (Fig. 12e). The $s_{u,DSS}$ of pre-strained Specimens OC-S and OC-L increased 16 and 50% compared to Specimen OC-0, respectively, the amount of which is commensurate with the degree of post-cyclic densification.

4. Concluding remarks

A series of constant-volume, monotonic and staged stress- and strain-controlled cyclic direct simple shear tests were conducted on intact and reconstituted, low and high plasticity silts to investigate evolution of cyclic resistance due to multiple dynamic loading events. The role of governing factors such as post-cyclic densification, apparent pseudo-

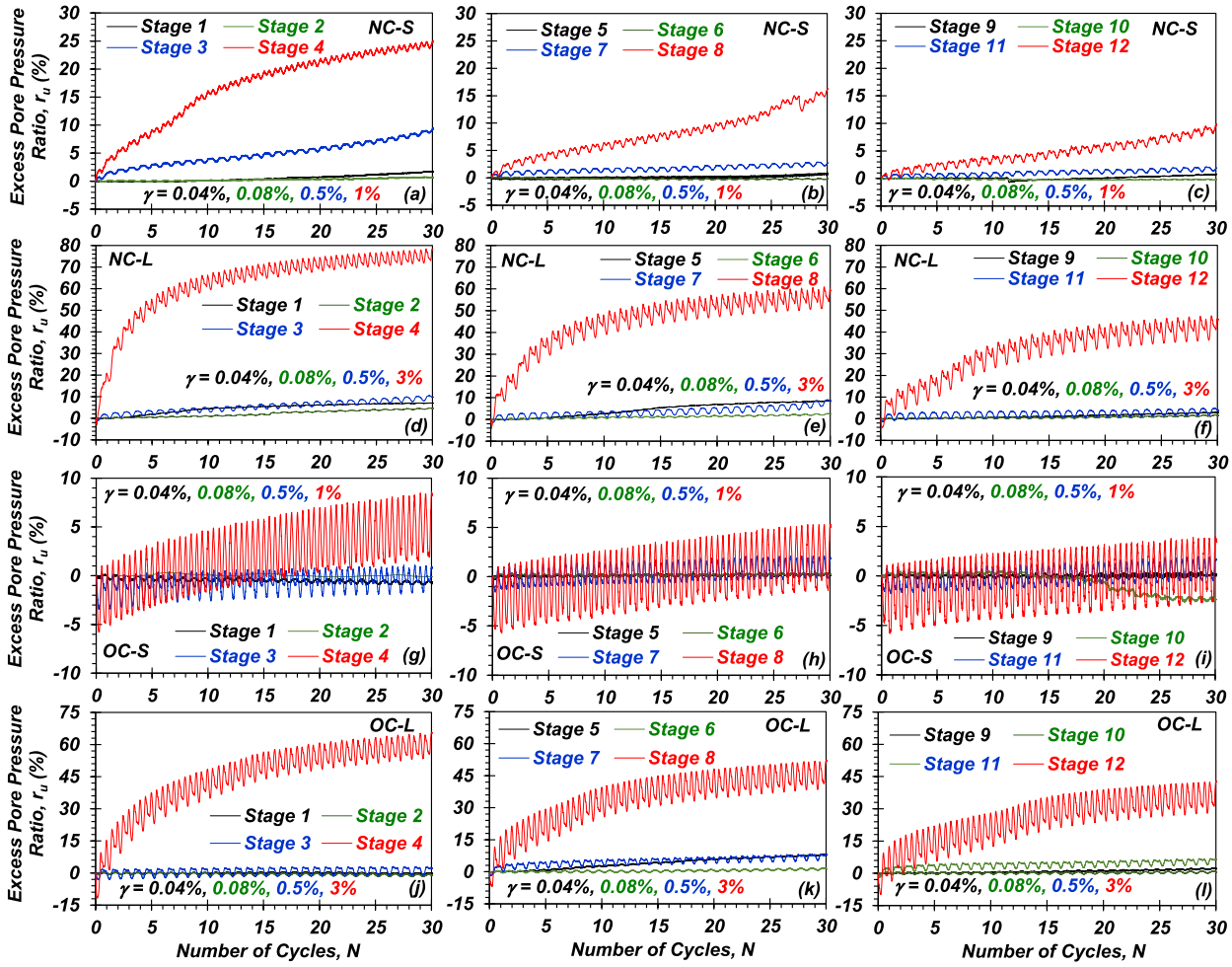

Fig. 11. Variation of excess pore pressure with *N* in staged, strain-controlled, cyclic DSS tests: (a–c) specimen NC-S, (d–f) specimen NC-L, (g–i) specimen OC-S, and (j–l) specimen OC-L.

overconsolidation, soil fabric, shear strain amplitude, potential bias in shear strain accumulation, and choice of failure criterion on the evolution of cyclic resistance have been investigated. The following conclusions may be drawn from the stress-controlled cyclic DSS tests:

- All specimens subjected to constant *CSR* throughout at least two shearing and reconsolidation stages exhibited a net increase in cyclic resistance ($N_{\gamma_{SA}=3.75\%}$) which is mainly attributed to the effect of increased dilation resulting from post-cyclic densification, increased pseudo-overconsolidation, rearrangement of soil particles resulting in improved particle interlocking, and a likely increase in lateral stress.
- Comparison of the cyclic resistance evaluated based on shear strain and excess pore pressure generation indicated notable inconsistencies. The evaluation of cyclic resistance is sensitive to the choice of failure strain criteria in subsequent stages of loading where specimens exhibit progressively increased density owing to the slower rate of shear strain accumulation.
- The symmetric accumulation of γ in the earlier loading stages does not guarantee a progressive increase in cyclic resistance based on a shear strain failure criterion, while the amplitude of γ_{max} developed can improve or degrade the cyclic resistance in subsequent stages, depending on its amplitude.
- Under constant *CSR,* intact specimens experienced smaller γ_{max} and reductions in void ratio compared to reconstituted specimens consolidated to similar effective stresses and *OCR*s, and gained greater cyclic resistance in terms of $N_{\gamma\ =\ 3.75}$.

The effect of pre-straining in terms of small and large shakings on the response of high plasticity reconstituted NC and OC silts was investigated using staged, strain-controlled, cyclic and post-cyclic monotonic tests on reconsolidated specimens to clarify the observations following stress-controlled testing. The following may be concluded:

- NC and OC specimens experiencing small and large shaking over multiple stages exhibited an overall increase in cyclic resistance indicated by generation of lower $r_{u,r}$. This observation implies that the detrimental effect of larger cyclic shearing was overridden by beneficial effects resulting from subsequent densification and cyclic stages with smaller shear strain amplitudes.
- Although the small pre-shaking did not change the density of the specimens significantly, it resulted in stronger soil fabric by removing local instabilities, increasing lateral stress, and adjustment in the arrangement of soil particles based on observed increases in V_s.
- The NC and OC specimens subjected to large shaking responded dramatically different than those under small shaking. The OC specimen exhibited reductions in cyclic resistance following the stage with the largest γ due to the presumable reduction of lateral stress and fabric destruction, followed by recovery in resistance in subsequent stages of small γ, until the next stage of large γ. The NC specimen exhibited progressive increases in cyclic resistance as a

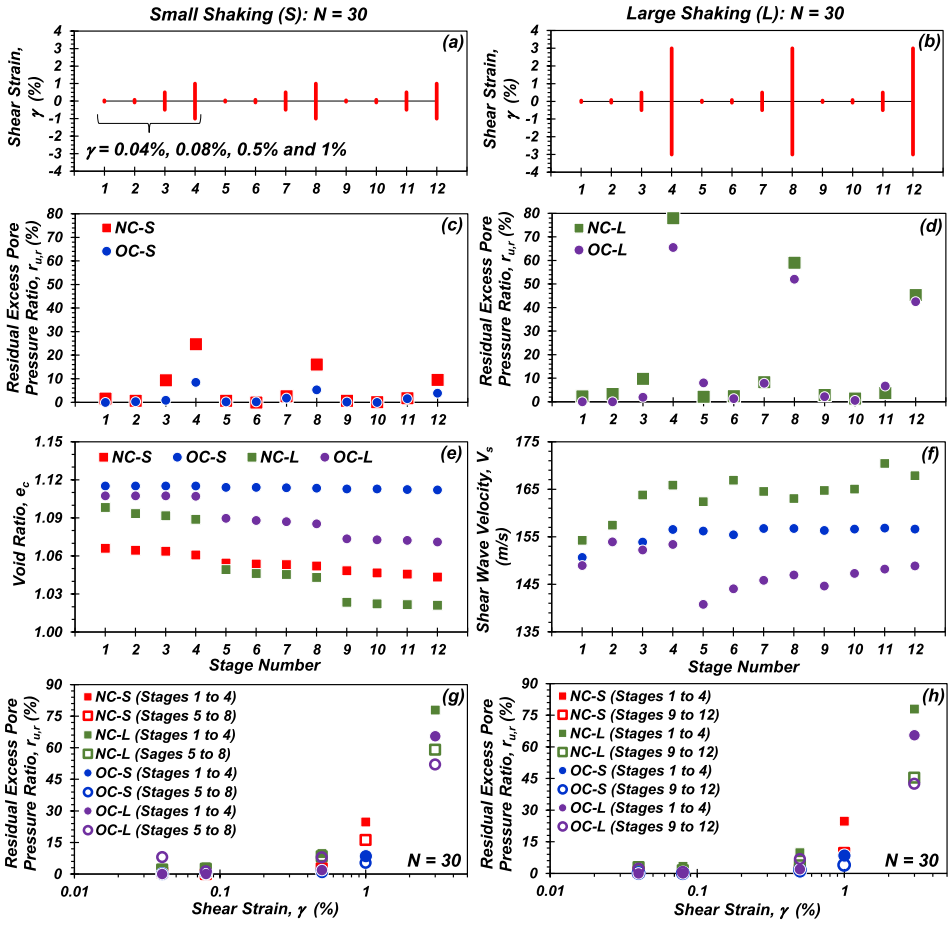

Fig. 12. Effect of magnitude of pre-shakings on excess pore pressure response and soil fabric of reconstituted NC and OC specimens of Site D: (a) and (b) schematic loading protocol for small and large pre-shakings, variation of: (c) and (d) residual excess pore pressure ratio for small and large shakings, respectively, (e) void ratio, and (f) shear wave velocity with stage numbers; variation of residual excess pore pressure ratio with shear strain for $N = 30$: (g) Stages 1–4 and 5 to 8 (small shakings), and (h) Stages 1–4 and 9 to 12 (large shakings).

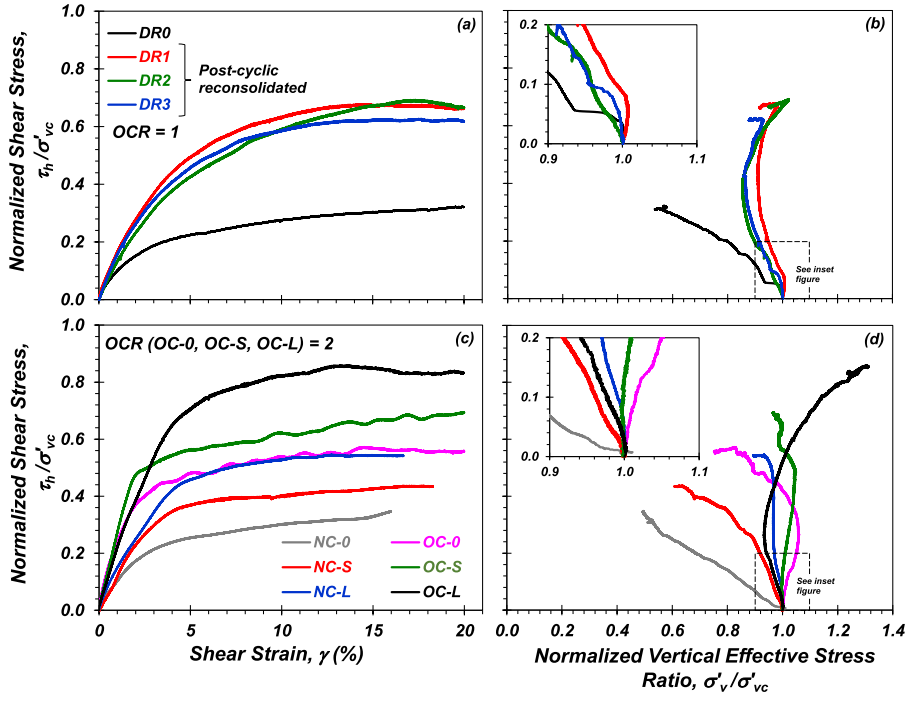

Fig. 13. Comparison of post-cyclic and virgin undrained DSS responses of reconstituted specimens including normalized shear stress-shear strain and effective stress paths: (a) and (b) staged, stress-controlled cyclic DSS tests, (c) and (d) staged strain-controlled cyclic DSS tests.

Table 6
Summary of undrained DSS tests results of specimens with and without cyclic loading history.

Test ID	Vertical Effective Consolidation Stress, $\sigma_{vc}^{'}$ (kPa)	*Initial OCR*	Void Ratio, e_c	Cumulative Post-cyclic Volumetric Strain in Previous Cyclic Loading, ε_{vpc} (%)	Maximum Shear Strain in Previous Cyclic Loading, γ_{max} (%)	Undrained Shear Strength Ratio, $s_{u,DSS}/\sigma_{vc}^{'}$
DR0	200	1.0	1.22	NA[1]	NA[1]	0.30
DR1	200	1.0	1.03	7.7	8.0	0.67
DR2	200	1.0	1.06	7.4	8.3	0.67
DR3	200	1.0	1.08	7.0	8.3	0.62
NC-0	200	1.0	1.12	NA[1]	NA[1]	0.33
NC-S	200	1.0	1.04	1.2	1.0	0.43
NC-L	200	1.0	1.01	4.2	3.0	0.54
OC-0	100	2.0	1.13	NA[1]	NA[1]	0.57
OC-S	100	2.0	1.11	0.2	1.0	0.66
OC-L	100	2.0	1.06	2.1	3.0	0.85

[1] NA = Not available.

result of densification, increasing pseudo-overconsolidation, and possible increase in lateral stress. It can be inferred that V_s is more sensitive to changes in fabric than changes in density for the specimens tested.

- The undrained shear strength of pre-strained specimens improved compared to virgin specimens due to post-cyclic densification, increased pseudo-overconsolidation (for NC specimens), and possible increases in lateral stress resulting from prior loading. Pre-strained specimens exhibited changes in volumetric tendencies relative to virgin specimens which varied with the strain amplitude during the cyclic stages. Changes in soil fabric following prestraining as inferred from shear wave velocity could not fully explain the changes in initial volumetric tendency under shear; however, the large strain monotonic behavior appeared to be controlled by post-cyclic densification.

Data availability statement

The data described herein are available for public access and use in the Next Generation Liquefaction Database (https://nextgenerationliquefaction.org/about/index.html).

Declaration of competing interest

The authors declare that they have no known competing financial interests or personal relationships that could have appeared to influence the work reported in this paper.

Acknowledgements

This material is based upon work supported by the National Science Foundation under grant CMMI-1663654. Any opinions, findings, and conclusions or recommendations expressed are those of the authors and do not necessarily reflect the views of the National Science Foundation. The writers wish to thank the anonymous reviewers for their helpful comments that served to improve the manuscript.

Appendix A. Supplementary data

Supplementary data to this article can be found online at https://doi.org/10.1016/j.soildyn.2022.107329.

References

[1] Cubrinovski M, Bradley B, Wotherspoon L, Green R, Bray J, Wood C, Pender M, Allen J, Bradshaw A, Rix G. Geotechnical aspects of the 22 february 2011 christchurch earthquake. Bull N Z Soc Earthq Eng 2011;44(4):205–26.
[2] van Ballegooy S, Malan P, Lacrosse V, Jacka M, Cubrinovski M, Bray J, O'Rourke T, Crawford S, Cowan H. Assessment of liquefaction-induced land damage for residential Christchurch. Earthq Spectra 2014;30(1):31–55.
[3] Kuribayashi E, Tatsuoka F. Brief review of liquefaction during earthquakes in Japan. Soils Found 1975;15(4):81–92.
[4] Youd TL, Bennett MJ. Liquefaction sites, Imperial Valley, California. J. Geotech. Eng. 1983;109(3):440–57.
[5] Holzer TL, Youd TL. Liquefaction, ground oscillation, and soil deformation at the Wildlife Array, California. Bull Seismol Soc Am 2007;97(3):961–76.
[6] El-Sekelly W, Dobry R, Abdoun T, Steidl J. Centrifuge modeling of the effect of preshaking on the liquefaction resistance of silty sand deposits. J Geotech Geoenviron Eng 2016;142(6):04016012.
[7] Finn W, Bransby PL, Pickering DJ. Effect of strain history on liquefaction of sand. J Soil Mech Found Div 1970;96(SM6).
[8] Andersen KH, Moussa AA. "Cyclic loading simple shear tests on sand". Internal Report: Norwegian Geotechnical Institute; 1973, 51501-1.
[9] Bjerrum L. Geotechnical problems involved in foundations of structures in the North Sea. Geotechnique 1973;23(3):319–58.
[10] Ishihara K, Okada S. Effects of stress history on cyclic behavior of sand. Soils Found 1978;18(4):31–45.
[11] Oda M, Kawamoto K, Suzuki K, Fujimori H, Sato M. Microstructural interpretation on reliquefaction of saturated granular soils under cyclic loading. J Geotech Geoenviron Eng 2001;127(5):416–23.
[12] Andersen KH. Cyclic soil parameters for offshore foundation design. In: Meyer V, editor. 3rd McClelland lecture: frontiers in offshore geotechnics III. Oslo, Norway: Taylor & Francis Group; 2015. p. 5–82.
[13] Sharp MK, Dobry R, Abdoun T. Liquefaction centrifuge modeling of sands of different permeability. J Geotech Geoenviron Eng 2003;129(12):1083–91.
[14] Ha I-S, Olson SM, Seo M-W, Kim M-M. Evaluation of reliquefaction resistance using shaking table tests. Soil Dynam Earthq Eng 2011;31(4):682–91.
[15] Evans TM, Zhang N. Three-dimensional simulations of plate anchor pullout in granular materials. Int J GeoMech 2019;19(4):04019004.
[16] Zhang L, Evans TM. Investigation of initial static shear stress effects on liquefaction resistance using discrete element method simulations. Int J GeoMech 2020;20(7). 04020087.
[17] Lee KL, Albaisa A. Earthquake induced settlements in saturated sands. J Geotech Geoenviron Eng 1974;100. Proc Paper 10496).
[18] Olson SM, Obermeier SF, Stark TD. Interpretation of penetration resistance for back-analysis at sites of previous liquefaction. Seismol Res Lett 2001;72(1):46–59.
[19] Wahyudi S, Koseki J, Sato T, Chiaro G. Multiple-liquefaction behavior of sand in cyclic simple stacked-ring shear tests. Int J GeoMech 2016;16(5):C4015001.
[20] El-Sekelly W, Dobry R, Abdoun T, Steidl J. Two case histories demonstrating the effect of past earthquakes on liquefaction resistance of silty sand. J Geotech Geoenviron Eng 2017;143(6):04017009.
[21] Dobry R, Thevanayagam S, El-Sekelly W, Abdoun T, Huang Q. Large-scale modeling of preshaking effect on liquefaction resistance, shear wave velocity, and CPT tip resistance of clean sand. J Geotech Geoenviron Eng 2019;145(10): 04019065.
[22] Andersen KH, Rosenbrand WF, Brown SF, Pool JH. Cyclic and static laboratory tests on Drammen clay. J Geotech Eng Div 1980;106(5):499–529.
[23] Lai Y, Wang L, Hong Y, He B. Centrifuge modeling of the cyclic lateral behavior of large-diameter monopiles in soft clay: effects of episodic cycling and reconsolidation. Ocean Eng 2020;200:107048.
[24] White DJ, Doherty JP, Guevara M, Watson PG. A cyclic py model for the whole-life response of piles in soft clay. Comput Geotech 2022;141:104519.
[25] Soysa A, Wijewickreme D. Repeated cyclic shear loading response of reconstituted Fraser River silt. In: Proc., proceedings of the 7th international conference on earthquake geotechnical engineering, rome, Italy; 2019.
[26] Wijewickreme D, Soysa A, Verma P. Observations on the response of natural fine-grained soils with respect to particle fabric. In: Proc., earthquake geotechnical engineering for protection and development of environment and constructions: proceedings of the 7th international conference on earthquake geotechnical engineering. Rome, Italy: CRC Press; 2019. p. 335. *ICEGE 2019), June 17-20, 2019*.
[27] Price A, DeJong J, Boulanger R. Cyclic loading response of silt with multiple loading events. J Geotech Geoenviron Eng 2017;143(10):04017080.
[28] Sanin M. Cyclic shear loading response of Fraser River Delta silt. M. ASc." thesis. The University of British Columbia; 2005.

[29] Wijewickreme D, Soysa A, Verma P. Response of natural fine-grained soils for seismic design practice: a collection of research findings from British Columbia, Canada. Soil Dynam Earthq Eng 2019;124:280–96.
[30] Dobry R, Abdoun T. Recent findings on liquefaction triggering in clean and silty sands during earthquakes. J Geotech Geoenviron Eng 2017;143(10):04017077.
[31] Dyvik R, Lacasse S, Berre T, Raadim B. Comparison of truly undrained and constant volume direct simple shear tests. Geotechnique 1987;37(1):3–10.
[32] ASTM D8296-19. Standard test method for consolidated undrained cyclic direct simple shear test under constant volume with load control or displacement control. West Conshohocken, PA: ASTM; 2019.
[33] Landon MM, DeGroot DJ, Sheahan TC. Nondestructive sample quality assessment of a soft clay using shear wave velocity. J Geotech Geoenviron Eng 2007;133(4):424–32.
[34] Jana A, Stuedlein AW. Monotonic, cyclic and post-cyclic response of an alluvial plastic silt deposit. J Geotech Geoenviron Eng 2021;147(3):04020174.
[35] Dadashiserej, A., Jana, A., Oritz, S.C., Walters, J.J., Stuedlein, A., Evans, T.M. "Monotonic, cyclic, and post-cyclic response of Willamette River silt at the van buren Bridge." 2022 *GeoCongress*, ASCE, Reston, VA. 12 pp.
[36] Jana A, Donaldson AM, Stuedlein AW, Evans TM. Deep, *in-situ* nonlinear dynamic testing of soil with controlled blasting: instrumentation, calibration, and example application to a plastic silt deposit. Geotech Test J 2021;44(5):GTJ20190426.
[37] Jana A, Stuedlein AW. Dynamic, in-situ, nonlinear-inelastic response and post-cyclic strength of a plastic silt deposit. Can Geotech J 2021;59(1). https://cdnsciencepub.com/doi/10.1139/cgj-2020-0652.
[38] Jana A, Stuedlein AW. Dynamic, in-situ, nonlinear-inelastic response of a deep, medium dense sand deposit. J Geotech Geoenviron Eng 2021;147(6):04021039.
[39] ASTM-D1587. Standard practice for thin-walled tube sampling of fine-grained soils for geotechnical purposes. West Conshohocken, PA: ASTM; 2015.
[40] Soysa A, Wijewickreme D. Comparison of cyclic shear response of three natural fine-grained soils having different plasticity. In: Proc., proc. Of the 16th world conference on earthquake engineering; 2017. *Santiago, Chile, paper*.
[41] Soysa AN. Monotonic and cyclic shear loading response of natural silts. *Ph.D. dissertation*, Dept. of Civil Engineering, Univ. of British Columbia; 2015.
[42] Krage CP, Price AB, Lukas WG, DeJong JT, DeGroot DJ, Boulanger RW. Slurry deposition method of low-plasticity intermediate soils for laboratory element testing. Geotech Test J 2020;43(5).
[43] ASTM D7928. Standard test method for particle-size distribution (gradation) of fine-grained soils using the sedimentation (hydrometer) analysis". West Conshohocken, PA, USA: ASTM International; 2017.
[44] Stokoe KH, Roberts JN, Hwang S, Cox BR, Menq F. Effectiveness of inhibiting liquefaction triggering by shallow ground improvement methods: field shaking trials with T-Rex at one area in Christchurch, New Zealand. In: 24th geot. Conf. Of torino, turin, Italy; 2016.
[45] Stokoe KH, Santamarina JC. Seismic-wave-based testing in geotechnical engineering. In: ISRM international symposium. OnePetro; 2000.
[46] Boulanger RW, Idriss IM. Liquefaction susceptibility criteria for silts and clays. J Geotech Geoenviron Eng 2006;(11):1413–26.
[47] Bray JD, Sancio RB. Assessment of the liquefaction susceptibility of fine-grained soils. J Geotech Geoenviron Eng 2006;132(9):1165–77.
[48] Armstrong RJ, Malvick EJ. Practical Considerations in the use of liquefaction susceptibility criteria. Earthq Spectra 2016;32(3):1941–50.
[49] Landon ME, Marchetti C, DeGroot DJ. Constant rate of strain consolidation testing of saturated cohesive soils without back pressure saturation. Geotech Test J 2018;41(2):425–33.
[50] ASTM-D-4186. Standard test method for one-dimensional consolidation properties of saturated cohesive soils using controlled-strain loading. West Conshohocken, PA: ASTM; 2012.
[51] Becker D, Crooks J, Been K, Jefferies M. Work as a criterion for determining in situ and yield stresses in clays. Can Geotech J 1987;24(4):549–64.
[52] Casagrande A. The determination of pre-consolidation load and it's practical significance. *Proc., Proc. Int. Conf. Soil Mech. Found. Eng.* Cambridge, Mass. 1936;60.
[53] DeJong JT, Krage CP, Albin BM, DeGroot DJ. Work-based framework for sample quality evaluation of low plasticity soils. J Geotech Geoenviron Eng 2018;144(10):04018074.
[54] Ladd CC. Stability evaluation during staged construction. J. Geotech. Eng. 1991;117(4):540–615.
[55] Grozic JLH, Lunne T, Pande S. An oedometer test study on the preconsolidation stress of glaciomarine clays. Can Geotech J 2003;40(5):857–72. https://doi.org/10.1139/t03-043.
[56] Grozic JLH, Lunne T, Pande S. Reply to the discussion by Clementino on "An oedometer test study on the preconsolidation stress of glaciomarine clays. Can Geotech J 2005;42(3):975–6. https://doi.org/10.1139/t05-011.
[57] Boone SJ. A critical reappraisal of 'preconsolidation pressure' interpretations using the oedometer test. Can Geotech J 2010;47(3):281–96.
[58] Umar M, Sadrekarimi A. Accuracy of determining pre-consolidation pressure from laboratory tests. Can Geotech J 2017;54(3):441–50.
[59] Boulanger RW, Idriss IM. Magnitude scaling factors in liquefaction triggering procedures. Soil Dynam Earthq Eng 2015;79:296–303.
[60] Wijewickreme D, Dabeet A, Byrne P. Some observations on the state of stress in the direct simple shear test using 3D discrete element analysis. Geotech Test J 2013;36(2):292–9.
[61] Leroueil S, Tavenas F, Brucy F, La Rochelle P, Roy M. Behavior of destructured natural clays. J. Geotech. Geoenviron. Eng., ASCE 1979;105(6):759–78.
[62] Høeg K, Dyvik R, Sandbækken G. Strength of undisturbed versus reconstituted silt and silty sand specimens. J Geotech Geoenviron Eng 2000;126(7):606–17.
[63] Long M, Vaid YP, Sivathayalan S. Strength of undisturbed versus reconstituted silt and silty sand specimens". discussion and closure. J Geotech Geoenviron Eng 2001;127(11):991–4.
[64] Wijewickreme D, Sanin M. Postcyclic reconsolidation strains in low-plastic Fraser river silt due to dissipation of excess pore-water pressures. J Geotech Geoenviron Eng 2010;136(10):1347–57.
[65] Zhu JF, Zhao HY, Jeng D-S. Effects of principal stress rotation on wave-induced soil response in a poro-elastoplastic sandy seabed. Acta Geotech. 2019;14(6):1717–39.
[66] Leonards GA, Ramiah BK. Time effects in the consolidation of clays. In: *Papers on soils 1959 meetings*, STP254-EB, 116–130. West Conshohocken, PA: American Society for Testing and Materials; 1960.
[67] Wagner N, Largent M, Stewart JP, Beyzaei C, Murphy D, Butkovich J, Egan JA. Stress history–dependent secondary compression of san francisco bay region old bay clays. J Geotech Geoenviron Eng 2021;147(7):04021045.
[68] Dahl KR, DeJong JT, Boulanger RW, Pyke R, Wahl D. Characterization of an alluvial silt and clay deposit for monotonic, cyclic, and post-cyclic behavior. Can Geotech J 2014;51(4):432–40.
[69] Idriss IM, Boulanger RW. Soil liquefaction during earthquakes." Monograph MNO-12. Oakland, CA: Erthquake Engineering Research Institute; 2008.
[70] Wijewickreme D, Soysa A. Stress–strain pattern–based criterion to assess cyclic shear resistance of soil from laboratory element tests. Can Geotech J 2016;53(9):1460–73.
[71] Darby KM, Boulanger RW, DeJong JT, Bronner JD. Progressive changes in liquefaction and cone penetration resistance across multiple shaking events in centrifuge tests. J Geotech Geoenviron Eng 2019;145(3):04018112.
[72] Boulanger RW, Idriss IM. Evaluation of cyclic softening in silts and clays. J Geotech Geoenviron Eng 2007;133(6):641–52. https://doi.org/10.1061/(ASCE)1090-0241(2007)133:6(641).